# ELECTRICAL RESISTIVITY IMAGING OF A COAL DEPOSIT AT TAI AREA OF GOMBE STATE, NORTH EASTERN NIGERIA

**BY**

**MOHAMMED MUSTAPHA ADEJO**

**M.Sc./SCI/42854/12-13**

**BEING A DISSERTATION SUBMITTED TO THE POSTGRADUATE SCHOOL,**

**AHMADU BELLO UNIVERSITY,**

**ZARIA, NIGERIA.**

**IN PARTIAL FULFILMENT FOR THE AWARD OF**

**MASTERS OF SCIENCE DEGREE IN APPLIED GEOPHYSICS**

**DEPARTMENT OF PHYSICS**

**FACULTY OF SCIENCE**

**AHMADU BELLO UNIVERSITY, ZARIA.**

**SEPTEMBER, 2015**

## DECLARATION

I declare that the work in this dissertation titiled “electrical resistivity imaging of a coal deposit at Tai area of Gombe state, north eastern Nigeria” has been carried out by me in the Department of Physics under the supervision of Prof. K. M. Lawal and Dr. A. L. Aminu. The information derived from the literature has been duly acknowledged in the text and a list of references provided. No part of this thesis was previously presented for another degree or diploma at this or any other institution.

**MOHAMMED, Mustapha Adejo**

| --- | --- | --- |
| Name of student | Signature | Date |

## CERTIFICATION

This dissertation titled **ELECTRICAL RESISTIVITY IMAGING OF A COAL DEPOSIT AT TAI AREA OF GOMBE STATE, NORTH EASTERN NIGERIA"** meets the regulations governing the award of degree of Masters of Science (M.Sc.) of Ahmadu Bello University, Zaria, and is approved for its contribution to knowledge and literary presentation.

| | | |
|---|---|---|
| Prof. K.M. Lawal | _____ | _____ |
| Chairman, Supervisory Committee | Signature | Date |
| Dr. A.L. Ahmed | _____ | _____ |
| Member, Supervisory Committee | Signature | Date |
| Dr. U. Sadiq | _____ | _____ |
| Head of Department | Signature | Date |
| Prof. Kabir Bala | _____ | _____ |
| Dean School of Postgraduate Studies | Signature | Date |

## DEDICATION

To my parents, Mal. Mohammed Adejo and Hajiya Salamatu Adamu

**ACKNOWLEDGEMENT**

First of all, I am indeed grateful to Almighty Allah, the Omnipotent, the Omniscience, for giving me the opportunity and strength to conclude my M.Sc. programme.

My profound gratitude goes to my Supervisors, Prof. K.M. Lawal and Dr. A.L. Ahmed for their technical guidance, constructive comments, critical reading and directions. I want to thank the Head of Department of Physics, Dr. U. Sadiq, P.G. coordinator, Dr. Y. Zakari, Seminar coordinator, Dr. M. Mamunu, Coordinator, Applied Geophysics unit, Dr. P. Sule and Chief Technologist, Mal. Bashir for their efforts in ensuring a successful running of the M.Sc. progamme.

My sincere appreciation goes to Mal. Sa'ad of SASCO Limited through whom I got to know about the study area and he also made all resources needed for the work at my disposal. I want to thank the Director, Centre for Geodesy and Geodynamics (CGG), Toro, Bauchi State, Dr. Tahir Abubakar Yakubu and the Head of Department of Earth Dynamics of (CGG), Mal. Muhammad Dalha.

I appreciate the efforts of my lecturers, Dr. P. Sule, Dr. K.M. Lawal, Dr. A.L. Ahmed, Mal. J. Raimi and Mr. J. Osumeje, for the quality knowledge of Geophysics they exposed me to.

I am grateful to Dr. H. Hamza, Dr. Y. Abubakar, Dr. Lawal, Prof. S.A. Alagbe and other lecturers in Geology for their intellectual contribution towards the actualization of the work and for the quality knowledge of Geology they exposed me to.

Special thanks to my senior colleagues: Yusuf Bello Ayoola, Bala Balarabe, Larry Bagudu, Sani Dahiru, Yusuf Avamiku, Adamu Abubakar, Mahmood Umar and others for the

support and solidarity they showed in ensuring the completion of this programme. I wish you all successful undertakings in your future endeavours.

To my parents, Mal. Mohammed Adejoh and Hajiya Salamatu Adamu, who sponsored this progamme, I ask Allah to reward them abundantly and engulf them with His mercy, grant them success both in this world and in the hereafter.

More modestly though, there are many people who have contributed in various ways to my completion of this dissertation and in as much as I would like to "observe protocol," the list is almost certainly endless, such is my debt of gratitude.

## ABSTRACT

A 2-D electrical resistivity imaging of some parts of Tai in Akko Local Government area of Gombe State, northeastern Nigeria was carried out. Tai is located 28km from Pindiga and lies between latitudes $10^0$ 00′00″ and $10^0$ 06′00″N and longitudes $10^0$ 40′ 00″E and $10^0$45′00″E. This study was prompted by a report that in the course of siting a hand-dug well and motorized borehole in Tai, coal seam was intercepted at a depth of about 18m. The aim of this geoelectrical investigation was to image the survey area for possible location and future exploitation of coal seams found in the area. The survey was targeted at determining the lateral extent of the coal seam, strike direction and resistivity values associated with the coal seams. The lund imaging system consisting of the ABEM Terrameter SAS 1000, electrode selector ES 464, stainless steel electrodes, multicore cables and jumpers was used to acquire the data in this survey. The protocol chosen was the Wenner-Schlumberger array because of its sensitivity to both horizontal and vertical structures, larger median depth of investigation and slightly better horizontal coverage. Data processing was done using RES2DINV software. The results show that the resistivity values range from 3Ωm to 2033Ωm. The top layer has resistivity ranges of about 66Ωm to 907Ωm. Below this, is a layer of low resistivity ranging from 3Ωm to 57Ωm probably saturated with water. The layer with resistivity range of 250Ωm to 900Ωm is probably the host of the coal seams. It can be concluded that the occurrence of the coal seam is probably more at the Northwest of the survey area and the coal seam is suspected to have resistivity values ranging from about 250Ωm to 900Ωm. It can also be inferred that the coal seam is striking in the Northeast-Southwest direction.

## TABLE OF CONTENTS


| | | Page |
|---|---|---|
| **TITLE PAGE** | | i |
| **DECLARATION** | | ii |
| **CERTIFICATION** | | iii |
| **DEDICATION** | | iv |
| **ACKNOWLEDGEMENT** | | v |
| **ABSTRACT** | | vii |
| **TABLE OF CONTENTS** | | viii |
| **LIST OF TABLES** | | xiii |
| **LIST OF FIGURES** | | xiv |
| **CHAPTER ONE: INTRODUCTION** | | 1 |
| 1.1 | General Overview | 1 |
| 1.2 | Statement of the Problem | 3 |
| 1.3 | Justification of the study | 3 |
| 1.4 | Aim and Objectives | 4 |
| 1.5 | Location of the study Area | 4 |

1.6 Climate and Vegetation 4

1.7 Geology of the Area 7

**CHAPTER TWO: LITERATURE REVIEW** 9

2.1 Previous Geophysical and Geological Investigations of Coal 9

2.2 Brief History of Coal 10

2.3 How Coal Is Formed 12

2.4 Types of Coal 13

2.5 Coal and the Environment 14

**CHAPTER THREE: MATERIALS AND METHOD** 16

3.1 Instrumentation 16

3.1.1 The ABEM Lund Imaging System 16

3.2 Electrical Resistivity Method 18

3.2.1 Theory of the Resistivity Method 20

3.2.2 Vertical Electrical Sounding (VES) 25

3.2.3 Constant Separation Traversing 26

3.3 Factors affecting Electrical Resistivity 26

3.3.1 Water Salinity 27

3.3.2 Porosity of Rock 27

3.3.3 Effect of Temperature 28

3.3.4 Effects of Rock Texture and Porosity 28

3.3.5 Effect of Geological Processes 29

3.4 The Concept of Apparent Resistivity 30

3.5 Typical Resistivity Values of Earth Materials 31

3.6 Reconnaissance Survey 35

3.7 Field Measurement Procedure 35

3.8 Choice of the Method 39

3.9 Field Problems 39

**CHAPTER FOUR: FIELD RESULTS AND INTERPRETATION** 41

4.1 Data Processing Procedure 41

4.2 Interpretation Technique 42

4.3 Field Results 44

4.3.1 Profile One 49

4.3.2 Profile Two 49

4.3.3 Profile Three 52

4.3.4 Profile Four 52

4.3.5 Profile Five 55

4.3.6 Profile Six 55

4.3.7 Profile Seven 58

4.3.8 Profile Eight 58

4.3.9 Profile Nine 61

4.4 Merging of the Profiles for the detection of continuity 63

**CHAPTER FIVE: DISCUSSION, CONCLUSION AND RECOMMENDATIONS** 65

5.1 Discussion 65

5.2 Conclusions 66

5.3 Recommendations 67

References 68

## LIST OF TABLES

Table 3.1: Coordinates of start points, midpoints and end points along the profiles. 37

## LIST OF FIGURES

Figure 1.1 Road Map from Zaria to the study area 5

Figure 1.2 Geological map of the Study Area (Tai) 6

Figure 3.1 ABEM Lund Imaging System together with Terrameter SAS 1000, ES 464 and other Accessories 19

Figure 3.2 Current and Potential Distributions within Homogeneous Isotropic Ground 20

Figure 3.3 A Typical Range of Resistivities of Geologic Materials (ABEM Instruction Manual, 2010) 33

Figure 3.4 Resistivities of Rocks, Soils and Minerals (Loke, 2004) 34

Figure 3.5 A Map Illustrating the profile layout 38

Figure 4.1 An example of a profile showing data set with a few bad data points 42

Figure 4.2 Arrangement of the blocks used in a model together with the data points in the pseudosection. 47

Figure 4.3 The result of 2D inversion of the Wenner- Schlumberger array data along profile one 50

Figure 4.4 The result of 2D inversion of the Wenner- Schlumberger array data along profile two 51

Figure 4.5 The result of 2D inversion of the Wenner- Schlumberger array data along profile three 53

Figure 4.6 The result of 2D inversion of the Wenner- Schlumberger array data along profile four 54

Figure 4.7 The result of 2D inversion of the Wenner- Schlumberger array data along profile five 56

Figure 4.8 The result of 2D inversion of the Wenner- Schlumberger array data along profile six 57

Figure 4.9 The result of 2D inversion of the Wenner- Schlumberger array data along profile seven 59

Figure 4.10 The result of 2D inversion of the Wenner- Schlumberger array data along profile eight 60

Figure 4.11 The result of 2D inversion of the Wenner- Schlumberger array data along profile nine 62

Figure 4.12 Resistivity model sections of all the profiles 64

# CHAPTER ONE: INTRODUCTION

## 1.1 General Overview

Coal is an organic sedimentary rock that forms from the accumulation and preservation of plant materials buried millions of years ago, usually in a swamp environment. Coal is the world's most abundant and widely distributed fossil fuel with reserves for all types of coal estimated to be about 990 billion metric tons, enough for 150 years at current consumption (BGR, 2009). Coal fuels 42% of global electricity production, and is likely to remain a key component of the fuel mix for power generation to meet electricity demand, especially the growing demand in developing countries (C.I.A.B., 2008). Estimates based on preliminary investigation reveals that Nigeria has an estimated coal reserve of over 2.7 billion tones (Sada, 2012). Despite the reported occurrence of these amounts of deposits, Nigerian Government has paid just little attention to coal exploration and according to World Coal Institute (2009), many countries like Poland, South Africa, China, and Australia rely on coal for over 94%, 92%, 77%, and 76% of its electricity respectively.

In the Gombe area of the Upper Benue Trough, the poorly developed coalfields occur within the Gombe Sandstone, which is of Maastrichtian age. The coals probably occur towards the bottom of the Gombe sandstone and are thought to be younger than the Enugu-Orukpa fields. The coals in Gombe area were intercepted at shallow depths of about 15m to 35m. The seams are generally thin, though one seam was reported to be up to 2m thick (Obaje, 2009).

Geophysical technique has been found very useful in many areas such as mineral exploration, groundwater investigation and some environmental studies. It involves studying the physical properties of the earth to provide vital information on subsurface

material conditions for numerous practical applications. These are done by taking measurements at or near the earth's surface that are influenced by the internal distribution of physical properties. Consequently, analysis of these measurements can reveal how the physical properties of the earth's interior vary vertically and laterally that reflect the subsurface geology. Another method of investigating subsurface geology is of course by drilling and pitting which provide information only at discrete locations and are expensive. Geophysical investigations are non-intrusive and non-invasive, thus avoiding the disruption caused by intrusive investigations such as drilling and pitting. Geophysical investigations cover large site areas rapidly and optimize the targeting of necessary intrusive inspections. In environments where intrusive investigations are not permissible, geophysics is the only answer. The methods employed include gravity, magnetics, seismic, resistivity, induced polarization, self potential, radiometrics, ground penetrating radar, electromagnetic methods, etc. These methods are cost effective and capable of detecting and delineating local features of interest.

The method employed for this research was the 2D Electrical Resistivity imaging, using the ABEM LUND Imaging System. The reason for adopting this method for this research is because from previous work, like the work of Singh *et al*. (2004) reveals that Coal seams have high resistivity with respect to the surrounding formation and its values vary from few hundreds of Ωm to few thousand Ωm. Their results suggest that this method can be applied to detect coal deposit. Also coal itself usually has a high resistivity compared to other sedimentary rock types. This property has formed the basis for detecting coal from borehole logs and DC resistivity surveying was used as a tool for exploring for coal as early as 1934 (Ewing *et al*., 1936).

Resistivity surveys determine the variation in the electrical resistivity of the subsurface by applying electric current across arrays of surface electrodes (Loke, 1999). Electrical resistivity is a function of porosity, fluid saturation, resistivity of the pore fluid and the solid, and the material texture among others. The survey data are processed to produce graphic depth sections of the thickness and resistivity of the subsurface electrical layers. All resistivity methods employ an artificial source of current, which is introduced into the ground through point electrodes or long line contacts; the latter arrangement is rarely used nowadays. The procedure is to measure potentials at other electrodes in the vicinity of the current flow. Because the current is measured as well, it is possible to determine an effective or apparent resistivity of the subsurface (Telford *et al*., 1976).

### 1.2 Statement of Problem

There was a report on the study area that in the course of digging a hand-dug well and also a hand-pump borehole, coal seams were intercepted at a depth of about 18m from the earth surface. Hence, the need to characterize the coal within the study area in terms of its lateral extends and strike direction.

### 1.3 Justification

Coal has important uses worldwide. The most significant uses are in electricity generation, steel production, cement manufacturing and other industrial processes. As a result of the aforementioned uses, the report of the occurrence of coal deposit within the area necessitates a geophysical investigation to ascertain the probable lateral extent and strike direction of the coal deposit in the area of study which will serve as a guide for an in-depth survey to ascertain the coal reserve of the area.

## 1.4 Aim and Objectives

The aim of the survey is to conduct electrical resistivity investigation around the study area where the coal deposit was intercepted so that inference can be made elsewhere in order to help in future exploration and exploitation of the coal deposit.

The objectives of this study are to determine the;

i. probable lateral extent of the coal deposit within the area and
ii. resistivity value associated with the coal seam.
iii. strike direction of the coal seam

## 1.5 Location of the Study Area

The area of study Tai, is in Akko Local Government area of Gombe State. Figure 1.1 depicts the topographical map of Tai and its environs. It lies between latitude $10^0$ 00′00″N and $10^0$ 06′00″N and longitude $10^0$ 40′ 00″E and $10^0$45′00″E. Figure 1.2 shows the geological map of the study area.

## 1.6 Climate and Vegetation

The study area falls within the semi-arid zone and is characterized by alternating wet and dry season. The highest daily temperature is about 38ºC which corresponds to the hottest period usually experienced in the months of March to April and the months of December to January are usually very cold with temperature as low as 25ºC. The dry season falls between October and April while the rainy season that is controlled by two contrasting wind systems (A warm and wet wind, and dry and cold wind) starting from May to September. The vegetation in the area is a typical Sudan Savannah characterized by high shrubs intervened with tall trees like mango, neem, locus trees, etc.

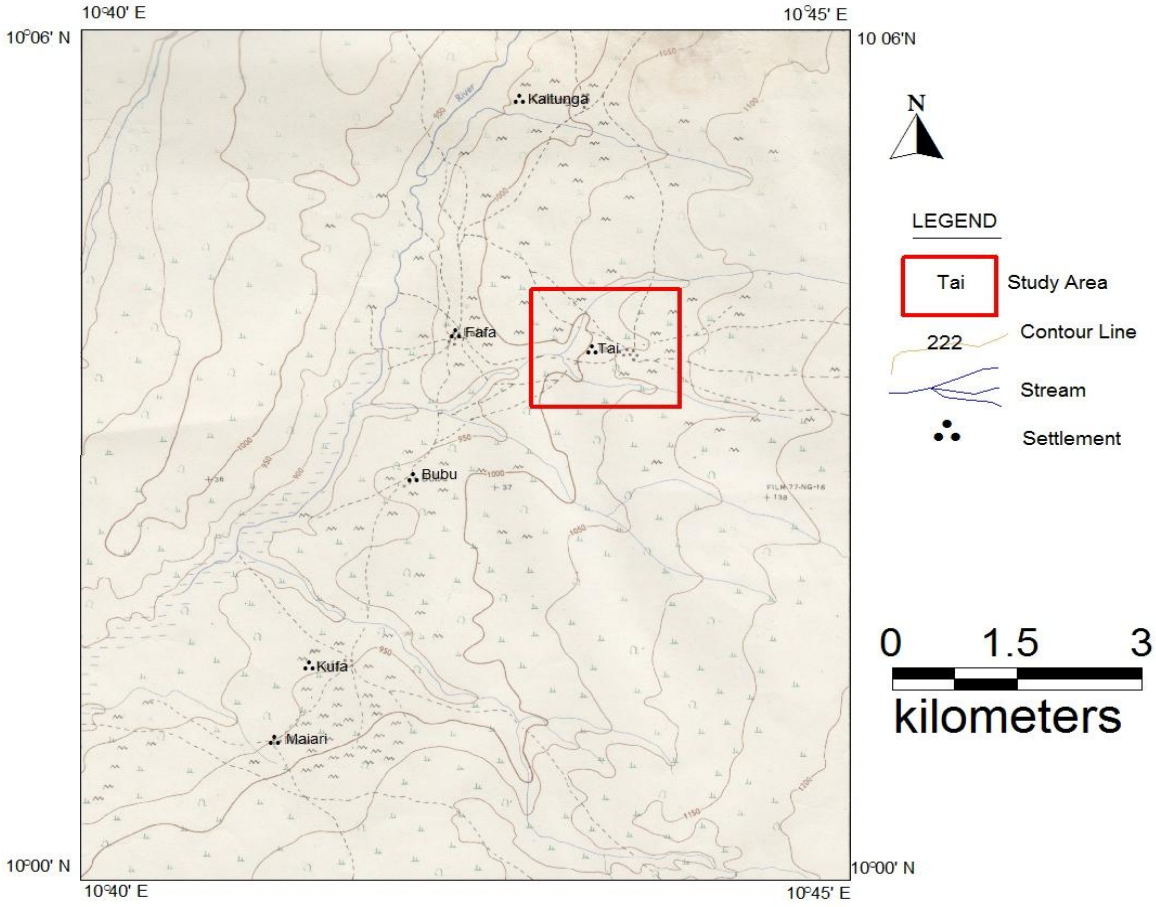
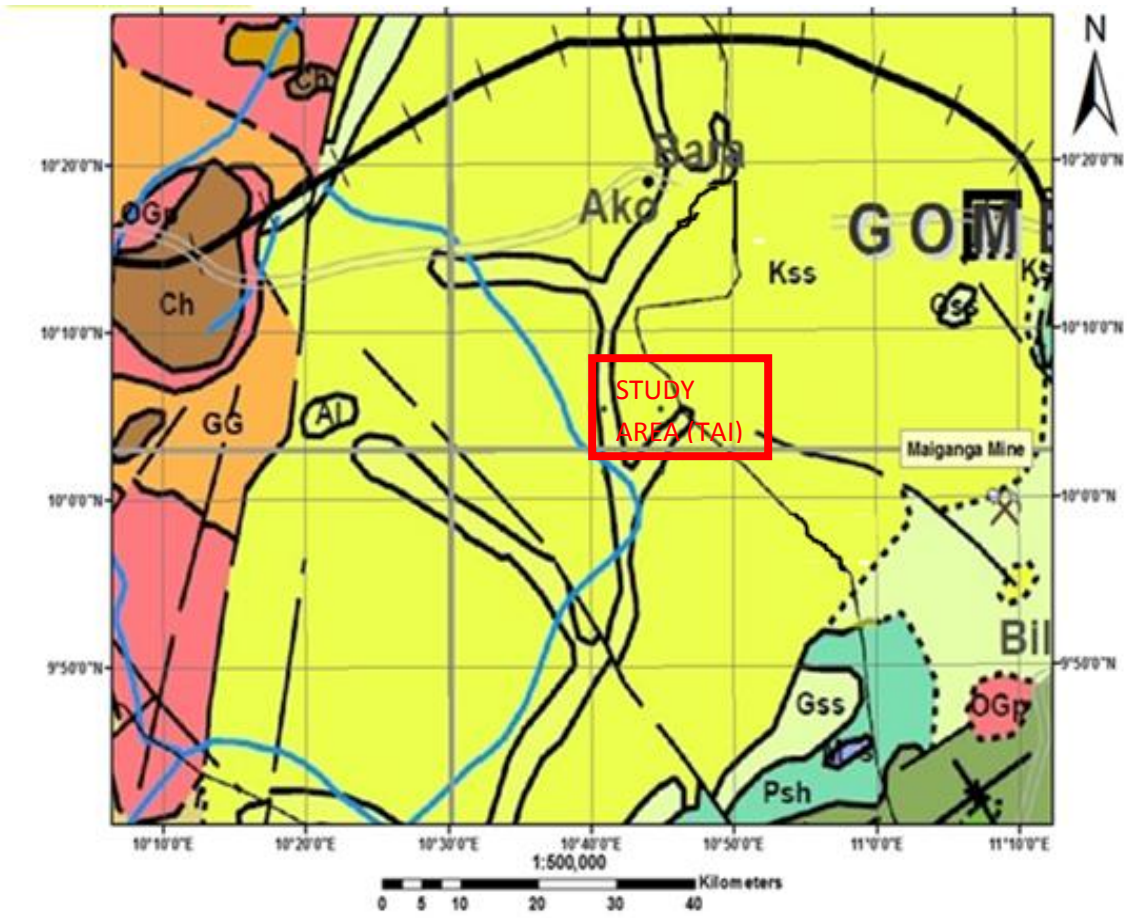



Fig. 1.1 Topographical Map of Tai and Its Environs




| | | | |
|---|---|---|---|
| Kss | Kerri-Kerri Formation | | Road |
| Gss | Gombe Sandstone | Tai | Study Area |
| Psh | Pindiga Formation | | River |
| OGP | Porphyritic Granite | | |
| Ch | Charnockitic Rocks | | |
| G G | Granite Gneiss | | |

Figure 1.2 Geological map of the study area (Courtesy Nigeria Geological survey)

## 1.7 Geology of the Area

The study area (Tai) forms part of the Upper Benue Trough which is made up of two arms, the Gongola Arm and the Yola Arm (although some authors have sub-divided the Upper Benue Trough to include a third central Lau-Gombe sub-basin, Akande *et al.*,1998). In both arms of the basin, the Aptian-Albian Bima Sandstone lies unconformably on the Precambrian Basement. This formation was deposited under continental conditions (fluvial, lacustrine) and is made up of coarse to medium grained sandstones, intercalated with clays, shales, and mudstones (Obaje, 2009). The Yolde Formation lies conformably on the Bima Sandstone. This formation of Cenomanian age represents the beginning of marine incursion into this part of the Benue Trough. The Yolde Formation was deposited under a transitional/coastal marine environment and is made up of sandstones, limestones, shales, clays and claystones. In the Gongola Arm, the Pindiga Formation lies conformably on the Yolde Formation. This formation represents full marine incursion into the Upper Benue Trough during the late Cenomanian marine transgression. Lithologically, this formation is characterized by the dark/black carbonaceous shales and limestones, intercalating with pale coloured limestones, shales and minor sandstones. The type locality of the Pindiga Formation is at Pindiga village. The Pindiga Formation is subdivided into three members namely: Kanawa, Deba-Fulani and Fika Members in the Gombe Sub-basin (Zaborski *et al.*, 1997). Post-folding sediments are represented by the continental Gombe Sandstone of Maastrichtian age and the Kerri–Kerri Formation of Tertiary age. The Gombe Sandstone is lithologically similar to the Bima Sandstone, attesting to the reestablishment of the Albian palaeoenvironmental condition (Obaje, 2009). The Gombe Sandstone however, contains coal, lignite, and coaly shale intercalations which in places are very

thick. The type locality of the Gombe Sandstone is along the bank of Pantami River in Gombe town. Good exposures are also encountered in many parts of Gombe town and Birin Fulani village (Obaje, 2009).

# CHAPTER TWO: LITERATURE REVIEW

## 2.1 Previous Geophysical Investigation of Coal

There is no record of any geophysical survey carried out in the present study area.

Ehinola *et al.* (2012) carried out vertical electrical sounding (VES) to identify the areal extent of coal and evaluated the coal thickness in Ute area, Ondo State. They have reported that the identified zone of interest (the coal horizon) has undergone a level of subsidence probably due to effect of tectonics and the reserve volume of coal computed is $1.02 \times 10^7$ metric tons.

Oladapo *et al*. (2008) adopted the electrical resistivity method utilizing the Schlumberger electrode configuration to study coal deposit at Unwana/Afikpo area of southern Nigeria. The result of the electrical resistivity study has revealed that the coal seams are predominant on the northeastern flank of the area of their study with possible coal occurrence outside that area.

Multielectrode resistivity imaging method was used by Singh *et al*. (2004) to study the coal seam located in the northern part of Jharia coal field of Dhanbad district, India. They have reported that the coal seam has a high resistivity range of 989Ωm to 1632Ωm at depths varying between 10m to 31m from the surface.

Johnson *et al.* (2003) carried out a survey using electrical resistivity method to detect underground coal mine voids with a pole-pole configuration of 20m electrode spacing in Lexington/Kentucky, United States. The result of their survey indicated that sufficient resolution was not obtained. The results did not appear to have any relationship to the coal

seam. But it was noted that the highest resistivity was immediately above the anticipated coal pillar.

Electrical resistivity method has been used for a similar geophysical survey. Though, the aim was not to target the coal seam, rather for the detection of voids where coal had been mined. Some of these works are;

Krishnamurthy *et al.* (2009) used electrical resistivity imaging (ERI) in one of the coal mining sites near Dhanbad to find out the barrier thickness and the water logged area in underground coal mines. Their result clearly indicated the water bearing zone along the profile which was well confirmed with the existing water level in the nearby bore wells. On the other hand, this technique did not identify the size of the coal pillar and gallery (air filled voids), which might be due to the small size of the voids (i.e. about 2m x 2m) below a depth of 15m and more but have indicated altogether as a high resistive zone ranging from 600Ωm to 1000Ωm.

Sheets (2002) has carried out a survey in Ohio, United States using electrical resistivity method to find out if he could identify areas where coal was mined, leaving air or water-filled voids. Several highly resistive areas were identified using dipole-dipole and Wenner resistivity surveys. Subsequent drilling and excavation led to the discovery of several air-filled abandoned underground mine tunnels.

**2.2 Brief History of Coal**

Coal has been a source of energy for almost as long as Homo sapiens have inhabited the planet. The earliest record for its use dates back more than 3000 years to China where it might have been used to smelt copper (C.E.C., 2012). In areas where coal seams intersected the surface, coal was a ready supply of energy just waiting to be exploited. It

did have some drawbacks, though. Most of the coal near the surface burns dirty, requiring some form of chimney if it is to be used indoors. It is also heavy to transport, limiting its use to regions near the source. Because of this, the use of coal through history was fairly sporadic. There is evidence for its use in Iron Age Britain, as well as in Rome near the beginning of the Common Era (Simon, 1995).

In North America in what is now the U.S. Southwest, the Hopi Indians during the 1300s used coal for cooking, heating and to bake the pottery they made from clay. Coal was later rediscovered in the United States by explorers in 1673. However, commercial coal mines did not start operation until the 1740s in Virginia (U.S.D.E., 2003). With improvements in mining, transportation, and ventilation in Medieval Europe, coal use gained in popularity. However, it was not until the beginning of the Industrial Revolution that coal use really took off. Large-scale manufacturing and transportation required tremendous amounts of energy, the likes of which wood could never supply without very quickly denuding every forest in Europe. Coal also had the advantage of being able to be used to make coke, which is used to manufacture steel. The invention of the coal-powered steam engine by James Watt enhanced the use of coal. It led to the train and the creation of the steam–powered boat, which made possible the quick and reliable transport of the manufacturing plants' goods to faraway locations.

In 1909, coal was first discovered in Enugu, Nigeria. The Ogbete drift mine opened six years later. The Ogbete mine's operations and others in the country were merged into a new corporation in 1950: The Nigerian Coal Corporation (NCC). The NCC was tasked with exploiting coal resources, (Nwaobi, 2005) and held a monopoly on coal and coke

mining, production, and sales until 1999. The NCC is hundred percent owned by the Federal Government and is headquartered in Enugu. NCC has operated two underground mines, Okpara and Onyeama, and two surface mines, Orukpa and Okaba, located on the eastern edge of the Anambra Coal Basin. Between 1950 and 1959, coal production in the Enugu mines increased annually from 583,487 tonnes to a peak of 905,397 tonnes (M.M.S.D., 2010). After 1959, production decreased significantly each year including the Civil War period of 1966 to 1970 when no coal production was reported.

Nigerian coal has been found suitable for boiler fuel, production of high calorific gas, domestic heating, briquettes, formed coke and the manufacture of a wide range of chemicals including waxes, resins, adhesives and dyes (M.M.S.D., 2010). Their characteristic properties (low sulfur and ash content and low thermoplastic properties), make these sub-bituminous coals ideal for coal-fired electric power plants. Some Nigerian coals can be used to produce formed-coke of metallurgical quality. The Gombe coal deposit is located east of Lafia-Obi. Preliminary drilling has indicated the presence of metallurgical grade coal, but no resource estimates have been made for this area (M.S.S.D., 2010).

**2.3 How Coal Is Formed**

Coal forms from the accumulation of plant debris, usually in a swamp environment, when plant debris dies and falls into the swamp. Swamp waters are usually deficient in oxygen, which would react with the plant debris and cause it to decay. This lack of oxygen allows the plant debris to persist. In addition, insects and other organisms that might consume the plant debris on land do not survive well under water in an oxygen deficient environment.

To form the thick layer of plant debris required to produce a coal seam the rate of plant debris accumulation must be greater than the rate of decay. Once a thick layer of plant debris is formed it must be buried by sediments such as mud or sand. These are typically washed into the swamp by a flooding river. The weight of these materials compact the plant debris and aids in its transformation into coal. About 10ft of plant debris will compact into just 1ft of coal (King, 2014). Plant debris accumulates very slowly. So, accumulating 10ft of plant debris will take a long time. The 50ft of plant debris needed to make a 5ft thick coal seam would require thousands of years to accumulate. During that long time the water level of the swamp must remain stable. If the water becomes too deep the plants of the swamp will drown and if the water cover is not maintained the plant debris will decay. To form a coal seam the ideal conditions of perfect water depth must be maintained for a very long time (King, 2014).

**2.4 Types of Coal**

Coal is classified into four main types or ranks (lignite, sub-bituminous, bituminous, anthracite), depending on the amounts and types of carbon it contains and on the amount of heat energy it can produce. The rank of a deposit of coal depends on the pressure and heat acting on the plant debris as it sank deeper and deeper over millions of years. For the most part, the higher ranks of coal contain more heat-producing energy.

Lignite is the lowest rank of coal with the lowest energy content. It has a carbon content of 25 to 35 percent and contains a lot of moisture, which lowers its heat value to between 4,000 and 8,000 Btu per pound (King, 2014). Lignite coal deposits tend to be relatively young coal deposits that were not subjected to extreme heat or pressure. It is mainly burned at power plants to generate electricity.

Sub-bituminous coal has a higher heating value than lignite. It only contains about 35 to 45 percent carbon, and its moisture content lowers its heating value to between 8,000 and 13,000 Btu per pound (King, 2014). These lower values are a result of sub-bituminous coal not being buried very deep in the ground. This coal is found very near to the surface, which means that it is produced through strip-mining.

Bituminous coal contains 45 to 86 percent carbon, and has two to three times the heating value of lignite (King, 2014). Bituminous coal is formed when a sub-bituminous coal is subjected to increased levels of organic metamorphism (i.e. under high heat and pressure). It is used to generate electricity and is an important fuel and raw material for the steel and iron industries.

Anthracite has the highest heating value and consists of between 86 to 98 percent carbon (King, 2014). When it is burned, it produces very little ash and pollutants other than carbon dioxide. From an energy use perspective, it is the highest grade. Its high carbon content means that anthracite coal experiences high temperatures and pressure during its existence, which points to most of it being found very deep in the earth.

**2.5 Coal And The Environment**

Environmental laws and modern technologies have greatly reduced coal's impact on the environment. Without proper care, mining can destroy land and pollute water. Today, restoring the land damaged by surface mining is an important part of the mining process. Because mining activities often come into contact with water resources, coal producers must also go to great efforts to prevent damage to ground and surface waters. When coal is burned as fuel, it gives off carbon dioxide, the main greenhouse gas that is linked with global warming (EIA, 2008). Burning coal also produces emissions, such as sulfur,

nitrogen oxide (NO), and mercury, that can pollute the air and water. Sulfur mixes with oxygen to form sulfur dioxide ($SO_2$), a chemical that can affect trees and water when it combines with moisture to produce acid rain. Emissions of nitrogen oxide help create smog, and also contribute to acid rain. Mercury that is released into the air eventually settles in water. The mercury in the water can build up in fish and shellfish, and can be harmful to animals and people who eat them. The Clean Air Act and the Clean Water Act require industries to reduce pollutants released into the air and the water. The coal industry has found several ways to reduce sulfur, nitrogen oxides, and other impurities from coal. They have found more effective ways of cleaning coal before it leaves the mine, and coal companies look for low-sulfur coal to mine. Power plants use "scrubbers" to clean sulfur from the smoke before it leaves their smokestacks (EIA, 2008). In addition, industry and government have cooperated to develop "clean coal technologies" that either remove sulfur and nitrogen oxides from coal, or convert coal to a gas or liquid fuel. The scrubbers and nitrogen oxide removal equipment are also able to reduce mercury emissions from some types of coal. Scientists are working on new ways to reduce mercury emissions from coal-burning power plants, since the Environmental Protection Agency (EPA) has set tighter mercury limits for the future.

# CHAPTER THREE: MATERIALS AND METHOD

## 3.1 Instrumentation

In resistivity measurement nowadays, there is a range of instrumentation from very simple to highly sophisticated equipment with the latter including the computer for infield data processing. The basic parts of any resistivity instrumentation are a portable power source which is either a D.C. or a low frequency A.C., Electrodes, preferably stainless steel electrodes and cables and reels, Global Positioning System (G.P.S.), meters for measuring current and voltage both of which may be combined in a single meter reading resistance or apparent resistivity. With the development of computer-controlled data collection and automatic data inversion, the use of computer-controlled multi-electrode systems with automatic measurement for the data acquisition became very relevant. This is because it gives a dramatic increase in field productivity. Such is the ABEM LUND Imaging System.

### 3.1.1 The ABEM Lund Imaging System

The LUND Imaging System is a multi-electrode system for cost effective and high resolution 2D and 3D resistivity surveys. It is an automatic electric imaging system suited for automatic resistivity profiling and drilling. The LUND Resistivity imaging System consists of a basic unit, a standard resistivity meter (ABEM Terrameter SAS 1000/4000) and a (4x64) multi-channel relay matrix switch unit called Electrode Selector ES 464. The system also has four multi-conductor electrode cables wound on reels each with 21 take-outs, stainless steel electrodes and cable jumpers and various connectors. The system is compatible with a portable PC-type computer or note book (laptop). Operating power comes from an internal 12 volts rechargeable NiCd battery pack. Model section plotting of 1D and 2D model interpretation sections in colour or gray scale including topography,

reference data and reference levels, utility software for extraction of VES, data manipulation and conversion, graphical output in PCX-file format *etc.*, are also available (ABEM instruction manual, 2010).

The Lund ES 464 basic system includes one ES 464 field unit with clip-on NiCd rechargeable battery pack and one communication cable from electrode selector to Terrameter. It is light weight and has waterproof, rugged cast aluminium casing. The Terrameter SAS system consists of a basic unit called the Terrameter SAS 1000/4000 and accessories like ES 464. It is a method whereby consecutive readings are taken automatically and the results are averaged continuously. Signal Averaging System (SAS) results are more reliable than those obtained from single-short systems. The SAS 1000 system (used in the present study) can operate in different modes, e.g., resistivity, self potential and induced polarization. In all its modes it is capable of measuring simultaneously in four channels thus making it suitable in all sorts of resistivity surveys.

The SAS 1000 is powered by a clip-on NiCd battery pack or by an external 12 volts source, which clips conveniently onto the bottom of the instrument. The SAS-EBA external 12 volts adapter allows the terrameter to utilize an external 12 volts D.C. source *e.g.*, a car battery. Stainless steel electrodes establish electric contact through long cables, to an ionic conductor which is the ground. All sorts of electrodes generate "noise". Noise is the fluctuating voltage that appears between a pair of electrodes placed so close that useful natural voltages are swamped. But stainless steel electrodes create less noise than electrodes made of ordinary steel. Current electrodes and potential electrodes make good contact with the ground to ensure low contact resistance and stability respectively (ABEM Instruction Manual, 2010).

The cables incorporate heavy gauge conductors with excellent insulation to ensure good survey results. The cables are expandable for deeper penetration by connecting them in series with cable joints. The cables have take-outs at 2m intervals along its length from which the cables are connected to the electrodes using cable jumpers having crocodile clips at both ends. The cables are wound on reels.

Figure 3.1 shows the basic instrumentation of the ABEM LUND Imaging System and accessories.

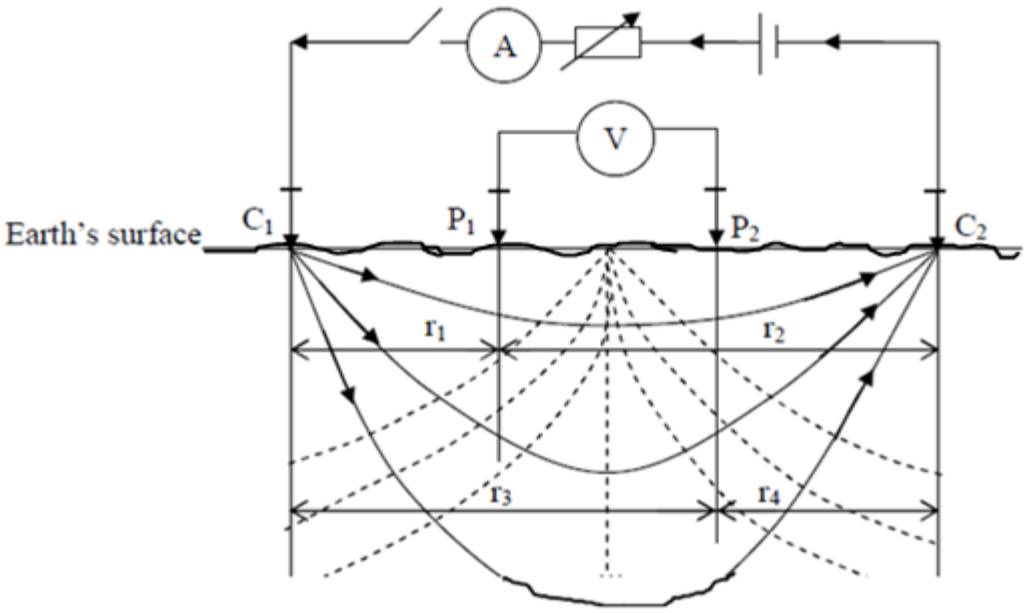
### 3.2 Electrical Resistivity Method

The resistivity method is based on measuring the electric potentials between one electrode pair while transmitting direct current (D.C.) between another electrode pair. The depth of penetration is inversely proportional to the separation between the electrodes in homogeneous ground. Varying the electrode separation provides information about the stratification of the ground.

Figure 3.2 shows the current and potential distributions within a homogeneous isotropic ground in a vertical plane through the current electrodes $C_1$ and $C_2$. When an external voltage is applied across them, there will be a flow of current through the earth from one electrode $C_1$ to the other, $C_2$. The resistivity method is based on measuring the potential between one electrode pair ($P_1$ and $P_2$, called potential electrodes) while transmitting D.C. between another electrode pair ($C_1$ and $C_2$) and $r_1$, $r_2$, $r_3$ and $r_4$ are the electrode separations. The rheostat varies the current I which is measured by the ammeter (A) while the voltmeter (U) measures the potential difference $\Delta U$.



Figure 3.1 ABEM LUND Imaging system




Current flow ⟶

Electric Potential ----------

Figure 3.2 Current ($C_1$, $C_2$) and Potential ($P_1$, $P_2$) Distributions within Homogeneous Isotropic ground.

### 3.2.1 Theory of the Resistivity method

The principle underlying the resistivity method is embodied in Ohm's law, which states that the current density at a given point is proportional to the electric field intensity at that point. Thus, Ohm's law gives the relationship between current density J (amperes/$m^2$) and electric field intensity E (volts/m) as:

$$J = \sigma E \tag{3.1}$$

where σ is the conductivity of the medium. Also E is the gradient of a scalar potential U (volts), i.e.,

$$E = -\nabla U \tag{3.2}$$

Putting equation (3.2) into equation (3.1)

$$J = -\sigma \nabla U \tag{3.3}$$

From divergence condition,

$$\nabla \cdot J = 0 \tag{3.4}$$

Thus, from equation (3.3)

$$\nabla \cdot J = -\nabla \cdot (\sigma \nabla U) = 0 \tag{3.5}$$

Or

$$\nabla \sigma \cdot \nabla U + \sigma \nabla^2 U = 0 \tag{3.6}$$

For a homogeneous earth, σ is a constant and since the derıvatıve of a constant is equal to zero, then the first term in equation (3.6) vanishes hence,

$$\nabla^2 U = 0 \tag{3.7}$$

Equation (3.7) is called Laplace's equation.

Applying relevant boundary conditions, equation (3.7) can be solved for specific cases. For instance, for a single current electrode buried deep in a homogeneous ground, equation (3.7) is expressed in spherical polar coordinates as:

$$\frac{1}{r^2}\frac{\partial}{\partial r}\left(r^2\frac{\partial U}{\partial r}\right)+\frac{1}{r^2\sin\theta}\frac{\partial}{\partial\theta}\left(\sin\theta\frac{\partial U}{\partial\theta}\right)+\frac{1}{r^2\sin^2\theta}\left(\frac{\partial^2 U}{\partial\phi^2}\right)=0 \qquad (3.8)$$

For a point current source, there is complete symmetry of current flow with respect to the **θ** and **ϕ** directions and the derivatives with respect to these directions are zero. Thus, equation (3.8) becomes

$$\frac{\partial}{\partial r}\left(r^2\frac{\partial U}{\partial r}\right)=0=\frac{d}{dr}\left(r^2\frac{dU}{dr}\right) \qquad (3.9)$$

Integrating equation (3.9) gives

$$r^2\frac{dU}{dr}=a \qquad (3.10)$$

Integrating equation (3.10) gives

$$U=-\frac{a}{r}+b \qquad (3.11)$$

where **a** and **b** are constants, U is the electric potential at the measuring point and r is the distance from that point to the single current electrode. Since U = 0 as $r\to\infty$ then b = 0 and

$$U=-\frac{a}{r} \qquad (3.12)$$

The current flows radially outwards in all directions from the point current electrode and the total current crossing a sphere of radius **r** is

$$I = 4\pi r^2 J = -4\pi r^2 \sigma \frac{dU}{dr} = -4\pi\sigma a = -\frac{4\pi a}{\rho} \tag{3.13}$$

after using equation (3.3) and equation (3.12). Thus,

$$a = -\frac{I\rho}{4\pi} \tag{3.14}$$

Putting equation (3.14) into equation (3.12) we have

$$U = \frac{I\rho}{4\pi}\frac{1}{r} \quad \text{Or} \quad \rho = 4\pi r\left(\frac{U}{I}\right) \tag{3.15}$$

The equipotentials which are everywhere perpendicular to the current flow lines will be spherical surfaces given by r is equal to a constant.

When the point current electrode of the three-point-system is located at the surface of the homogeneous isotropic medium and the air above has zero conductivity, the return current electrode is at a great distance. As in the previous case b=0 since U=0 as $r \to \infty$

In addition $\frac{\partial U}{\partial z} = 0$ at z = 0

since $\sigma_{air} = 0$. In the present case, all the current flows through a hemispherical surface in the lower region.

Hence

$$a = -\frac{I\rho}{2\pi} \quad \text{and} \quad U = \frac{I\rho}{2\pi}\frac{1}{r} \quad \text{or} \quad \rho = 2\pi r\left(\frac{U}{I}\right) \tag{3.16}$$

Thus generally, the potential difference between 2 arbitrarily located points on the surface of a homogeneous isotropic ground is given by the following expression.

$$\Delta U = \frac{I\rho}{2\pi}\left(\frac{1}{r_1} - \frac{1}{r_2} - \frac{1}{r_3} + \frac{1}{r_4}\right) \tag{3.17}$$

where **ρ** is the resistivity, **I** is the current and $r_1$, $r_2$, $r_3$, and $r_4$, are the inter-electrode distances as shown in Figure (3.3).

From equation (3.17) when the ground is inhomogeneous the apparent resistivity can be solved for as;

$$\rho = \rho_a = \frac{\Delta U}{I}\frac{2\pi}{\left(\frac{1}{r_1} - \frac{1}{r_2} - \frac{1}{r_3} + \frac{1}{r_4}\right)} \tag{3.18}$$

The result is independent of the position of the electrodes and is not affected when the current and the potential electrodes are interchanged.

The resistance is calculated using Ohm's law:

$$R = \frac{\Delta U}{I} \tag{3.19}$$

where **R** is the resistance in ohms; $\Delta U$ is the potential difference in volts; and **I** is the current in amperes.

The material parameter **ρ** which is the inverse of electrical conductivity **σ** is related to the resistance via a geometric factor **K′** that is a function of the electrode configuration. The resistivity of the homogeneous ground can be calculated using, the relation

$$\rho = K' \frac{\Delta U}{I} \tag{3.20}$$

$$\text{where } K' = \frac{2\pi}{\left(\frac{1}{r_1} - \frac{1}{r_2} - \frac{1}{r_3} + \frac{1}{r_4}\right)} \tag{3.21}$$

The electrical resistivity methods have been widely used for shallow and deep investigations, routinely in geothermal, mining, coal, groundwater and engineering applications (Keller and Frischknecht, 1966). Several researchers have proved the suitability and effectiveness of these methods by studying the response of diverse structures such as faults (Long, 1954; Bhattacharaya and Patra,1968; Apparao and Roy, 1971), dykes (Zohdy, 1969; Kumar, 1973), contacts (Stanley *et al*., 1976; Patella, 1978). In engineering application, electrical surveys are used for dam stability studies, bedrock strength, mapping of overburden, faults and fractures. Resistivity studies are often effective because the resistivity of porous earth material is primarily a function of the amount of fluid which fills the pores, the conductivity of fluid and the clay content of the matrix (Kean *et al.*, 1987). There are three basic modes of operation for any resistivity method: sounding, profiling and sounding-profiling.

### 3.2.2 Vertical Electrical Sounding (VES)

This is also known as electrical drilling or expanding probe. It is used mainly in the study of horizontal or near horizontal interfaces. In this method the current and potential electrodes are symmetrically expanded about a fixed central point. Consequently, readings are taken as the current reaches progressively greater depth.

The measured apparent resistivity values are normally plotted against electrode spacing values on a log–log graph paper. To interpret the data from such a survey, it is normally assumed that the subsurface consists of horizontal layers. In this case, the subsurface resistivity changes only with depth, but does not change in the horizontal direction.

In many engineering and environmental studies, the subsurface geology is very complex where the resistivity can change rapidly over short distances. The resistivity sounding method might not be sufficiently accurate for such situations. However, the technique is extensively used in geotechnical surveys to determine overburden thickness and also in hydrogeology to define horizontal zones of porous strata.

### 3.2.3 Constant Separation Traversing (CST)

This is also known as electrical profiling. It is used to determine lateral variations of resistivity. The current and potential electrodes are maintained at a fixed separation and the array is progressively moved along different profiles. This gives some information about lateral changes in the subsurface resistivity, but cannot detect vertical changes in the resistivity. This method is employed in mineral prospecting to locate faults or shear zones and to detect localized bodies of anomalous conductivity. It is also used in geotechnical surveys to determine variations in bedrock depth and the presence of steep discontinuities. Results from a series of CST traverses with fixed electrode spacing can be employed in the production of resistivity contour maps.

The most useful method is a combination of sounding and profiling which delineates both lateral and vertical variations in resistivity. This is the method employed in electrical imaging. The present study has made use of electrical imaging.

### 3.3 Factors Affecting Electrical Resistivity

The electrical resistivity of rocks and minerals is an extremely variable property and depends on a number of factors. Bulk resistivities from the surface to more than 15km depth in a normal crust are controlled by aqueous electrolytic conduction by way of pores, fractures, faults, and shear zones. The resistivity of crystalline rock formations such as granulites, granite, and diorite in situ is largely dependent upon the water in the fissures and fractures. Similarly, the porosity, degree of saturation and the nature of pore-electrolytes govern the resistivity of rocks like sandstone and limestone. A slight increase in resistivity with depth is the result of decreasing pore, fracture, fault and shear-zone porosity due to increased lithostatic load. Other hydrological factors are outlined below.

#### 3.3.1 Water Salinity

Conduction in near-surface rocks is largely electrolytic, taking place in connected pore spaces, along grain boundaries, in fractures, faults and shear zones but negligibly through the silicate framework (Keller and Frischknecht, 1966).

The ions which conduct the current result from the dissociation of salts, such dissociation occurring when salts are dissolved in water. Since each ion is able to carry only a definite quantity of charge, it follows that the more ions that are available in a solution the greater will be the charge that can be carried. Hence, the solution with the larger number of ions will have the higher conductivity. In general, for a given porosity, a rock which contains saline water within its pores will have a greater conductivity when the salinity of the water is high than when it is low. Resistivity decreases with increase in salinity.

#### 3.3.2 Porosity of Rock

Porosity can be defined as the ratio of the percentage of the volume of void space to the total volume of the rock. Porosity arises from the fact that the particles do not occupy all

the possible space. It provides a direct measure of the total void space available for the storage of fluids.

Resistivity and porosity in sedimentary rocks can be related by the general form of Archie's law, which for rocks devoid of clay is written as

$$F = \frac{\rho_r}{\rho_s} = a\phi^{-m} \tag{3.22}$$

where F is the formation resistivity factor, $\rho_r$ is the resistivity of the rock, $\rho_s$ is the resistivity of the solution in the pores of the rock, $\phi$ is porosity, while "a" and "m" are constants peculiar to the rock type. The constant "m" is usually referred to as the cementation factor while the constant "a" is referred to as the coefficient of saturation (Keller and Frischknecht, 1966).

The most common minerals forming soils and rocks have very high resistivity in a dry condition, and the resistivity of soils and rocks is therefore normally a function of the amount and quality of water in pore spaces and fractures. The degree of connection between the cavities is also important.

### 3.3.3 Effect of Temperature

An increase in temperature lowers the viscosity of water, with the result that ions in the water become more mobile. The increased mobility of the ions results in an observed resistivity decrease with increase in temperature according to the formula (Keller and Frischknecht, 1966):

$$\rho_t = \frac{\rho_{18^0}}{1+\alpha_t\left(t-18^0\right)} \tag{3.23}$$

where $\rho_{18^0}$ is the resistivity measured at a reference temperature of $18^0$C, $\alpha_t$ is the temperature coefficient of resistivity (about 0.025 per degree centigrade for most electrolytes) and t is the ambient temperature.

### 3.3.4 Effects of Rock Texture and Porosity

The texture of a rock dictates its resistivity in the following ways:

(i) A well-sorted sandstone has large void spaces and hence exhibits low resistivity.

(ii) A poorly-sorted sandstone will have a much lower porosity and hence will exhibit higher resistivity.

(iii) Dissolution along fractures in a limestone will enhance porosity and hence lower resistivity.

(iv) Precipitation of some minerals in any rock will lower the porosity and hence increase resistivity.

(v) Basalt has much unconnected or dead-end pore space and hence low permeability, so that even basalt of high porosity may exhibit high resistivity.

### 3.3.5 Effects of Geological Processes

In general, geological processes reduce the resistivity of a rock but there are exceptions. Weathering or hydrothermal alteration of a granite significantly lowers its resistivity. Dissolution, faulting and shearing usually increase porosity and fluid permeability, and hence lower resistivity. Precipitation of calcium carbonate and silica reduces porosity and hence reduces fluid permeability and increases resistivity. Induration by compaction or metamorphism will reduce porosity and permeability and hence increase resistivity. Salt water intrusion provides more ions for conduction and therefore reduces resistivity.

### 3.4 The Concept of Apparent Resistivity

Most resistivity techniques define a response function called apparent resistivity, $\boldsymbol{\rho_a}$ which can be calculated from the surface measurements. These apparent resistivities are usually functions of a variable that is related to the depth of current penetration.

The apparent resistivity is equal to the true resistivity only when the subsurface is homogeneous. In practice, this condition is difficult to obtain. However, the subsurface is assumed to be divided into thin strata with each stratum regarded as completely homogeneous and isotropic (Koefoed, 1979). This is a convenient way of representing a response of the actual distribution of lateral resistivity in the subsurface on the basis of subsurface measurements. If the electrodes are laid out along a profile and their separations are increased systematically, the change in the apparent resistivity will be a function of electrode spacing. Subsurface resistivity is measured by applying an electric current through two current electrodes and measuring the resulting voltage difference between potential electrodes. For the general four electrode spread, the potential difference $\Delta U$ between the potential electrodes is given by equation (3.17).

By measuring $\boldsymbol{\Delta U}$ and $\mathbf{I}$ and knowing the electrode configuration, the resistivity can be calculated. Over uniform earth or homogeneous isotropic medium this calculated resistivity is constant for different electrode separation and any current. However, if the ground is inhomogeneous, the calculated resistivity varies as the electrode spacing is varied or the array is moved about. This calculated resistivity is called "apparent resistivity $\rho_a$", which is diagnostic of the real resistivities of the subsurface in the vicinity of the electrode array. The apparent resistivity may be smaller or larger than the real resistivities or in rare cases identical with one of the real resistivity values. The apparent resistivity is

the same as the real resistivity in a homogeneous subsurface, but normally a combination of contributing strata of an inhomogeneous subsurface. The value of the apparent resistivity obtained with small electrode spacing is called the surface resistivity. In any electrode layout, the potential and current electrodes can be interchanged and from the principle of reciprocity, the apparent resistivity should be the same (unchanged) in either case.

### 3.5 Typical Resistivity Values of Earth Materials

Of all the physical properties of earth materials (rocks and minerals), electrical resistivity has the widest range of variation. Resistivity of metallic minerals may be as small as $10^{-5}\Omega$m. That of dry close-grained rocks like gabbro could be as large as $10^{7}\Omega$m (Telford *et al*., 1990). The maximum possible range is even greater, from native silver, $1.6\text{x}10^{-8}\Omega$m to pure sulphur $10^{16}\Omega$m. A good conductor is usually defined as a material of resistivity less than $10^{-5}\Omega$m while an insulator is one having resistivity greater than $10^{7}\Omega$m, between this limit lies the semi-conductors (Telford *et al*., 1990). The common minerals forming rocks and soils have very high resistivity values in dry condition and the resistivity of rocks and soils is therefore normally a function of the amount and quantity of water in pores and fractures. The degree of connection between cavities is also important; consequently the resistivity of a rock type or soil type may vary widely. The electrical resistivity varies between different geological materials depending mainly on variations in water content and dissolved ions in the water. Resistivity investigations can thus be used to identify zones with different electrical properties, which can then be referred to different geological strata. However, the variation may be limited within confined geological area and variations in resistivity within certain soil or rock type will reflect variations in

physical properties. For example the lowest resistivities encountered for sandstones and limestone mean that the pore spaces in the rock are saturated with water, whereas the highest values represent strongly consolidated sedimentary rock or dry rock above the groundwater surface (ABEM instruction manual, 2010).

Sand, gravel and sedimentary rocks may also have very low resistivities provided the pores in the rocks are saturated with saline water. Fresh crystalline rock is highly resistive apart from certain ore minerals, but weathering commonly produces highly conductive clay rich saprolite (ABEM instruction manual, 2010).

The variation in characteristics within one type of geological material makes it necessary to calibrate resistivity data against geologic documentation for instance, surface mapping, test pits or drilling. Typical ranges of resistivities of geologic materials are shown in Figures 3.3 and 3.4. The amount of water in a material depends on its porosity. Porosity may be divided into primary porosity and secondary porosity. Primary porosity consists of pore spaces between the mineral particles and occurs in soils and sedimentary rocks. Secondary porosity consists of fractures and weathered zones, and this is the most important porosity in crystalline rocks such as granites and gneisses. Secondary porosity may also be important in certain sedimentary rocks such as limestone. Even if the porosity is rather low, the electrical conduction taking place through water filled pore spaces may reduce the resistivity of the material drastically. The degree of water saturation will of course affect the resistivity, thus the resistivity above the groundwater level will be higher than below if the material is the same. Consequently, the method can be used to find the depth to groundwater in materials where a distinct groundwater table exists. However, if the content of fine grained material is significant, the water content above the groundwater

surface, held by hygroscopic and capillary forces may be large enough to dominate the electrical behaviour of the material. The resistivity of pore water is dominated by the concentration of ions in solution, the type of ions and the temperature. The presence of clay minerals strongly affects the resistivity of sediments and weathered rocks. The clay minerals may be regarded as electrically conductive particles which can absorb and release ions and water molecules on its surface through an ion exchange process. Very roughly, igneous rocks have the highest resistivity, sedimentary rocks the lowest and metamorphic rocks intermediate. However, there is a considerable overlapping. Resistivities of particular rock types vary with age and lithology, since the porosity of the rock and the salinity of the contained water are affected by both (ABEM instruction manual, 2010).

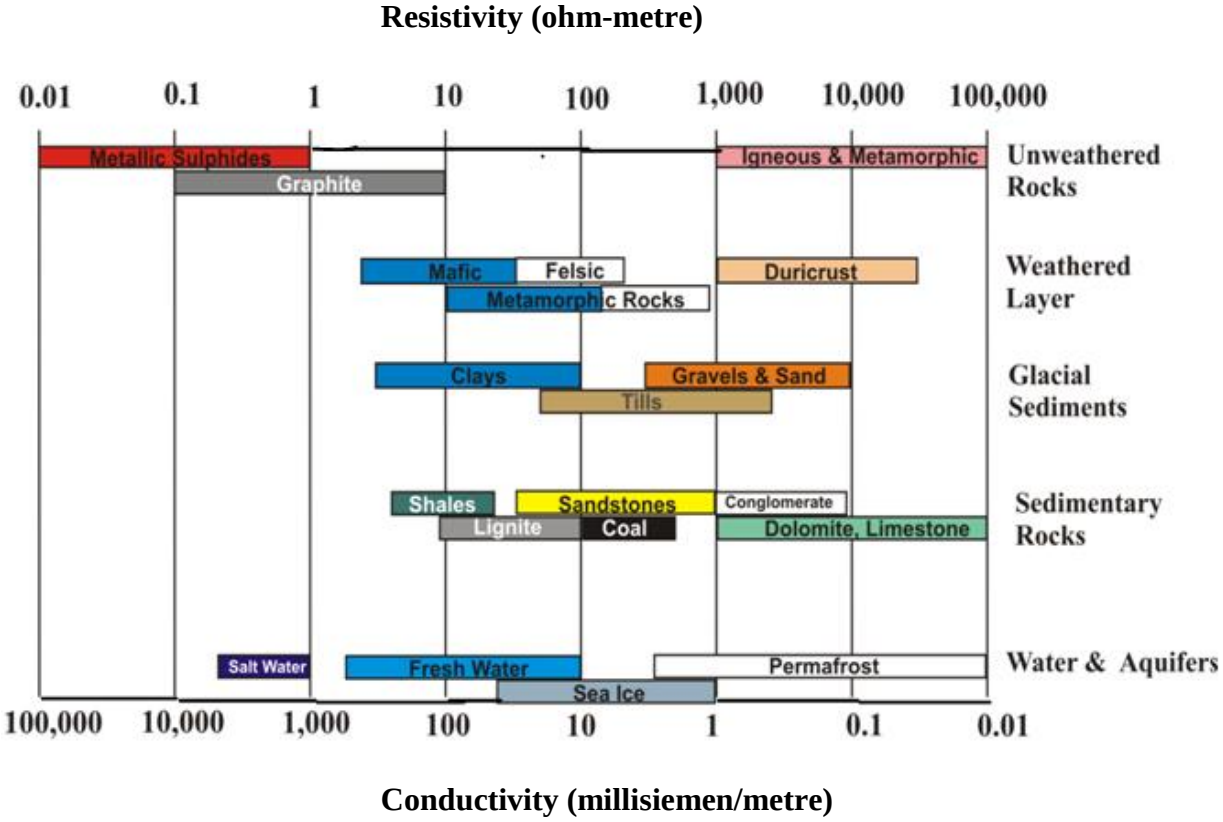



**Figure 3.3: A Typical Range of Resistivities of Geological Materials (ABEM Instruction Manual, 2010).**

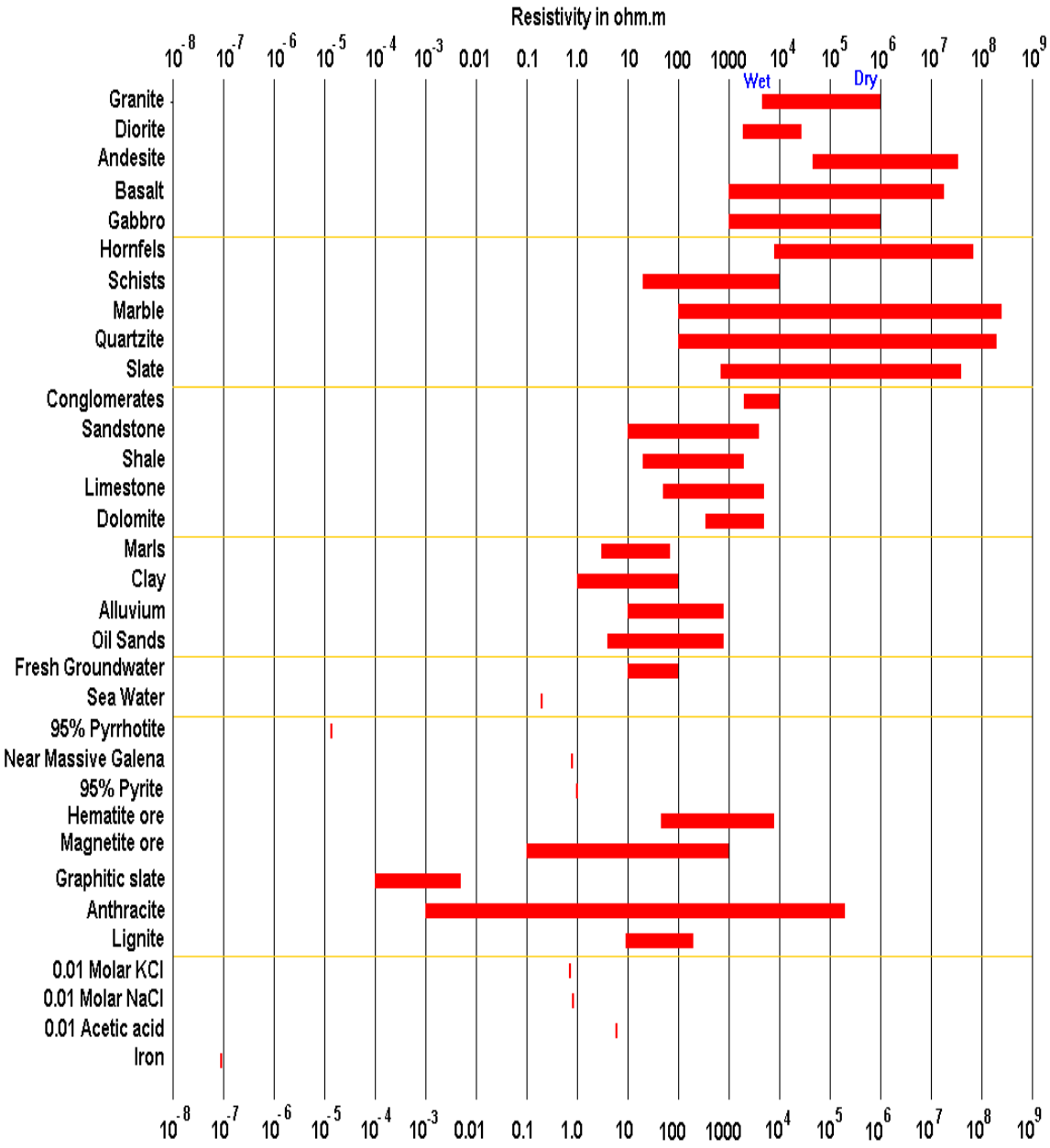



**Figure 3.4: Resistivities of Rocks, Soils and Minerals (Loke, 2004)**

### 3.6 Reconnaissance Survey

Topographical maps and geological maps were obtained. A walk around the entire area to be surveyed with these maps was made, to consider whether resistivity surveying was suitable for the current problem. It was discovered that the method was suitable. So possible profile lines were selected and the entire lengths of the planed profile lines were inspected to ensure their practicability before returning to the area for the detailed survey.

### 3.7 Field Measurement Procedure

Electrical Resistivity Imaging (tomography) is a method by which 2D images of subsurface resistivity distribution are generated (Batayneh, 2006). Using this method, features with electrical properties differing from those of the surrounding material may be located and characterized in terms of electrical resistivity, geometry and depth of burial. The electrical resistivity tomography data are collected using computer-controlled measurement systems connected to multi-electrode arrays. The data acquisition process is completely controlled by the computer software which checks that all the electrodes are connected and properly grounded before measurement starts. After adequate grounding is achieved the software scans through the measurement protocol selected. The Wenner-Schlumberger array was chosen for this survey. The field measurement usually started with laying out the cables and electrodes along the chosen profile. Each cable has 21 take-outs. The Terrameter SAS 1000 and the ES 464 were placed in the centre of the layout. The two cables were connected to the Electrode Selector (ES 464) at the centre of the layout. Take-out 1 of one cable and take-out 21 of the second cable were made to overlap at the cable ends and in the layout centre. The serial port of the Terrameter was connected to the Electrode Selector. The electrodes were connected to all the take-outs at intervals of 2m on the electrode cables using cable jumpers. For a moist or soft ground, electrodes

were just pushed into the ground by hand and then connected. However, hammering and wetting were done on dry and hard ground. The Terrameter was then connected to an external 12 volts battery and switched on, which automatically switches on the Electrode Selector and the system set-up which was echoed to the screen. The instrument was set to resistivity mode and LUND Imaging System was selected. Electrode test commenced immediately, and grounding improved for the electrodes with bad ground contact. The connectors were also checked for unsatisfactory electrode positions. Electrodes were tested pair-wise against each other starting from the outermost electrodes going towards the centre. The electrode test checks if it is possible to transmit current through all electrodes. This test takes a couple of minutes but saves time afterwards; because programme may stop depending on poor electrode contact. Measurement will also stop if the batteries for either the Terrameter or the Electrode Selector are low. The programme automatically continues to measure using the two electrode cables when the contact is satisfactory. It was ensured that measurements did not stop during the measurement period. As measurement continued apparent resistivity values were echoed on the screen. When measurement on each layout was finished, the programme was stopped and the Terrameter switched off. The cables were disconnected, wound up, and the electrodes and jumpers were all collected together. The instrument was then transferred to a new profile and the entire process was repeated until all the profiles were completed. While measuring the profiles, the positions of reference points along the lines were noted. The coordinates of the starting points, midpoints and end points of each of the profiles were noted to facilitate identification of points for further investigation (Table 3.1). Nine profiles were taken for the survey (Figure 3.5).

Table 3.1: Coordinates of start points, midpoints and end points along the profiles.

| S/N | Profile | Start Point | Mid Point | End Point |
|---|---|---|---|---|
| 1 | 1 | $N10^0$ 03′ 43.86″<br>$E10^0$ 43′ 28.68″ | $N10^0$ 03′ 43.20″<br>$E10^0$ 43′ 27.00″ | $N10^0$ 03′ 42.78″<br>$E10^0$ 43′ 25.92″ |
| | 2 | $N10^0$ 03′ 42.78″<br>$E10^0$ 43′ 26.04″ | $N10^0$ 03′ 41.70″<br>$E10^0$ 43′ 26.94″ | $N10^0$ 03′ 40.38″<br>$E10^0$ 43′ 27.66″ |
| | 3 | $N10^0$ 03′ 40.00″<br>$E10^0$ 43′ 27.60″ | $N10^0$ 03′ 40.80″<br>$E10^0$ 43′ 28.68″ | $N10^0$ 03′ 41.46″<br>$E10^0$ 43′ 29.70″ |
| | 4 | $N10^0$ 03′ 41.70″<br>$E10^0$ 43′ 29.76″ | $N10^0$ 03′ 42.72″<br>$E10^0$ 43′ 29.16″ | $N10^0$ 03′ 43.80″<br>$E10^0$ 43′ 28.80″ |
| | 5 | $N10^0$ 03′ 43.32″<br>$E10^0$ 43′ 30.42″ | $N10^0$ 03′ 41.52″<br>$E10^0$ 43′ 31.14″ | $N10^0$ 03′ 40.26″<br>$E10^0$ 43′ 31.86″ |
| | 6 | $N10^0$ 03′ 40.20″<br>$E10^0$ 43′ 31.86″ | $N10^0$ 03′ 40.38″<br>$E10^0$ 43′ 33.18″ | $N10^0$ 03′ 40.26″<br>$E10^0$ 43′ 34.62″ |
| | 7 | $N10^0$ 03′ 40.02″<br>$E10^0$ 43′ 34.56″ | $N10^0$ 03′ 41.34″<br>$E10^0$ 43′ 34.44″ | $N10^0$ 03′ 42.72″<br>$E10^0$ 43′ 34.32″ |
| | 8 | $N10^0$ 03′ 42.48″<br>$E10^0$ 43′ 33.84″ | $N10^0$ 03′ 42.36″<br>$E10^0$ 43′ 32.58″ | $N10^0$ 03′ 42.18″<br>$E10^0$ 43′ 31.20″ |
| | 9 | $N10^0$ 03′ 38.94″<br>$E10^0$ 43′ 35.64″ | $N10^0$ 03′ 40.32″<br>$E10^0$ 43′ 35.52″ | $N10^0$ 03′ 41.52″<br>$E10^0$ 43′ 35.70″ |




Figure 3.5: A map illustrating the profile layout (1 to 9). P1 and P2 are locations of hand dug well and hand-pump borehole. Arrows are indicating profiles direction.

### 3.9 Choice of the Method

In this work, Wenner-Schlumberger array was used. The Wenner-Schlumberger is a new hybrid between the Wenner and Schlumberger array arising out of more recent work with electrical imaging survey (Pazdirek and Blaha, 1996). This method was used for the following reasons:

1. It has a slightly better horizontal coverage compared with the Wenner array.

2. It is moderately sensitive to both horizontal and vertical structures. In area where both types of geological structures are expected, this array might be a good compromise between the Wenner and dipole-dipole array.

3. The median depth of investigation for this array is about 10% larger than that for the Wenner array for the same electrode spacing.

4. The signal strength for this array is weaker than that for the Wenner array, but it is higher than the dipole-dipole array and twice that of the pole-dipole (Loke, 2014).

### 3.9 Field Problems

Some of the problems encountered during the field measurement are as follows:

i. Draining of the battery during the field measurement slowed down the process because, the battery had to be recharged before measurements would be restarted or an alternative battery had to be provided which increased the expenses.

ii. Poor contact between the electrodes and ground when the electrodes were hammered vertically into the hard ground.

iii. Animals such as goats, sheep and cows moving around the field sometimes disrupted the measurements.

iv. The practical difficulty in moving great length of cables and electrodes around.

# CHAPTER FOUR: FIELD RESULTS AND INTERPRETATION

## 4.1 Data Processing Procedure

The measured apparent resistivity data files for all the resistivity imaging survey lines were downloaded from the ABEM ES464 Terrameter and burnt on a rewriteable compact disc. The disc was uploaded into a computer in which ABEM file conversion (SAS1000 Utilities) and RES2DINV application software have been installed. The SAS4000 Utilities software was used to convert the original data file (in .s4k format) to the appropriate (.DAT format) input file readable by the inversion software RES2DINV. A total of nine files were converted. Each of the converted file represented a profile which was imported into the Res2dinv programme. It is worth noting that to get a good model, the data must be of equally good quality. Therefore the apparent resistivity data were viewed as a profile plot showing each data level and inherent bad data points were eliminated (example shown Fig. 4.1). Even though great care was taken during the survey measurements, inherent bad data points were visible by their unique high or low values when compared to neighboring data points. The bad data points might have been generated from sources such as; very poor ground contact at an electrode such that sufficient current could not be injected into the ground; failure of the relays at one of the electrodes. Eliminating these data point were inevitable, otherwise they might influence the final output model.

The inversion of the input data set for each profile was carried out (after satisfactory data editing) with least-square inversion routine. The final output displayed after the inversion were the measured and calculated apparent resistivity pseudosections and the inverse model showing true depth and true formation resistivity. RES2DINV carried out the inversion.

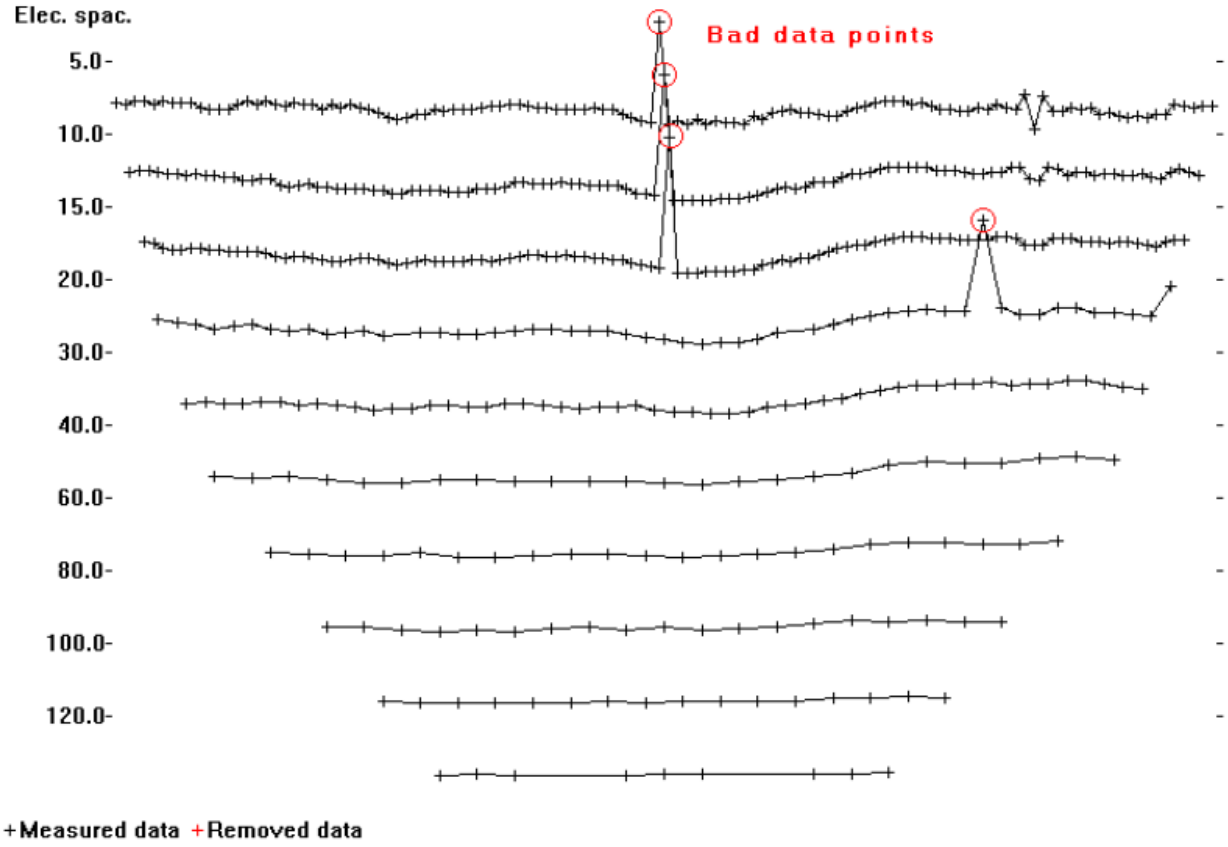



Fig 4.1 An example of a profile showing data set with a few bad data points

### 4.2 Interpretation Technique

Interpreting the resistivity data consists of two steps: a physical interpretation of the measured data, resulting in a physical model, and a geological interpretation of the resulting physical parameters (Dahlin, 2001). The large-scale VES data were interpreted with the state-of-the-art interpretation technique, called the 2D smoothed damped least-squares inversion algorithm. The results obtained based on 2D inversion of field data and borehole information, were interpreted to determine the depth and extent of shallow bedrock, thickness of overburden, aquifer, *etc*. In interpreting LUND Imaging data, Computer assistance is needed due to the large amount of data collected from the field.

The PSEUDO.EXE and ERIGRAPH.EXE software packages for instance have been used for the automatic drawing of pseudosections in grey scales or colour, using linear interpolating between data points. Third party software packages for resistivity data processing can also be used for advanced interpretation. One example of such a programme is RES2DINV.EXE, which performs smoothness constrained inversion (automatic model interpretation) using finite difference forward modelling and quasi-Newton techniques (Loke, 1999).

The true resistivity structure has been interpreted using automatic 2D smoothness constrained least-squares inversion. The smoothness constrain prevents unstable and extreme solutions, whereas a quasi-Newton technique reduces the numerical calculations (Loke and Barker, 1996). Quite often a useful amount of information can be extracted from a pseudosection by careful inspection of the contour pattern and apparent resistivity values, particularly if some geological control is available. Contours tend to follow horizontal or gently sloping boundaries between strata of different resistivities, though steep contacts are much smoothed. Steep boundaries can be identified using some of the gradient measurement provided they show a strong resistivity contrast. Contour peaks and troughs are correctly positioned relative to the subsurface features giving rise to them, and some estimate of depths at which boundaries occur may be made.

Hence, qualitatively speaking, the subsurface structure may be quite obvious though this is by no means always so. If there are marked departures from 'two dimensionality,' the contour pattern may be affected by resistivity contrasts close to, but outside the plane of the section. Such effects can lead to serious errors both at the qualitative and quantitative stages of interpretation. Also faulting can be difficult to detect due to the smoothing effect

of the Wenner array (Griffiths *et al*., 1990). Even if the acquisition of a data set is straightforward due to the improvements in resistivity devices, the interpretation involves many factors and can be difficult when some parameters in the inversion procedure are neglected. Such parameters include the stability, robustness and uniqueness of the inversion algorithm (Cardarelli and Fischanger, 2006).

### 4.3 Field Results

The raw field resistivity data were processed using RES2DINV software programme. RES2DINV is a computer programme designed by Loke (1994), to invert the apparent resistivity data obtained from electrical imaging surveys into a two-dimensional (2-D) true resistivity model of the subsurface with less input from the user. The inversion routine used by the programme is based on the smoothness-constrained least-squares method (de Groot-Hedlin and Constable 1990, Sasaki, 1992).The smoothness-constrained least-squares method is based on the following equation

$$(\mathbf{J}^T\mathbf{J} + u\mathbf{F})\mathbf{d} = \mathbf{J}^T\mathbf{g} \qquad (4.1)$$

where $\mathbf{F} = \mathbf{f}_x\mathbf{f}_x^T + \mathbf{f}_z\mathbf{f}_z^T$

$\mathbf{f}_x$ = horizontal flatness filter

$\mathbf{f}_z$ = vertical flatness filter

**J** = matrix of partial derivatives

u = damping factor

**d** = model perturbation factor

**g** = discrepancy vector

The forward problem is solved through a finite difference algorithm, whose main features are a versatile user-defined discretization of the domain and a new approach to the solution of the inverse Fourier transform. The forward modelling subroutine is used to calculate the apparent resistivity values. The inverse procedure is based on an iterative smoothness-constrained least-squares algorithm. This computer programme uses a smoothness constrained non-linear least-squares optimisation inversion technique to convert measured apparent resistivity values to true resistivity values and plot them as pseudosections.

The discrepancy vector, **g**, contains the difference between the calculated and measured apparent resistivity values. The magnitude of this vector is frequently given as a RMS (root-mean-squared) value. This is the quantity that inversion method seeks to reduce in an attempt to find a better model after each iteration. The model perturbation vector, **d**, is the change in the model resistivity values calculated using the above equation which normally results in an "improved" model. The above equation tries to minimize a combination of two quantities, the difference between the calculated and measured apparent resistivity values as well as the roughness (i.e., the reciprocal of the model smoothness) of the model resistivity values. The damping factor, **u**, controls the weight given to the model smoothness in the inversion process. The larger the damping factor, the smoother will be the model but the apparent resistivity RMS error will probably be larger.

One advantage of this method is that the damping factor and flatness filter can be adjusted to suit different types of data. The programme creates a resistivity cross-section, calculates the apparent resistivities for that cross-section, and compares the calculated apparent resistivities to the measured apparent resistivities. The iteration continues until a combined smoothness constrained objective function is minimized. The depth of investigation cannot

be determined by simple calculations and it depends on the acquisition geometry, the conductivity structures and data errors (Oldenburg and Li, 1999).

The 2D model used by the programme divides the subsurface into a number of rectangular blocks, to determine the resistivity of the rectangular blocks that will provide an apparent resistivity pseudosection that agrees with the actual measurements. For the Wenner and Schlumberger arrays, the thickness of the first layer of blocks is set at half times the electrode spacing. The arrangement of the blocks is loosely tied to the distribution of the data points in the pseudosection. The distribution and the size of the blocks are automatically generated by the programme, so that the number of blocks usually do not exceed the number of data points. The depth of the bottom row is set to be approximately equal to the equivalent depth of investigation (Edwards, 1977) of the data points with the largest electrode spacing. This arrangement is shown in Figure 4.2.

The RES2dinv programme uses a forward modelling subroutine (smoothness-constraint method) to calculate apparent resistivity values and a non-linear least squares optimization technique for the inversion routine. (de Groot-Hedlin & Constable, 1990). The optimization method basically tries to reduce the difference between the calculated and measured apparent resistivity values by adjusting the resistivity of the model blocks. A measure of this difference is given by the root-mean squared (RMS) error. However the model with the lowest possible RMS error can sometimes show large and unrealistic variations in the model resistivity values and might not always be the "best" model from a geological perspective. In general the most prudent approach is to choose the model at the iteration after which the RMS error does not change significantly and usually occurs between the 3rd and 5th iterations (RES2DINV, 2010).

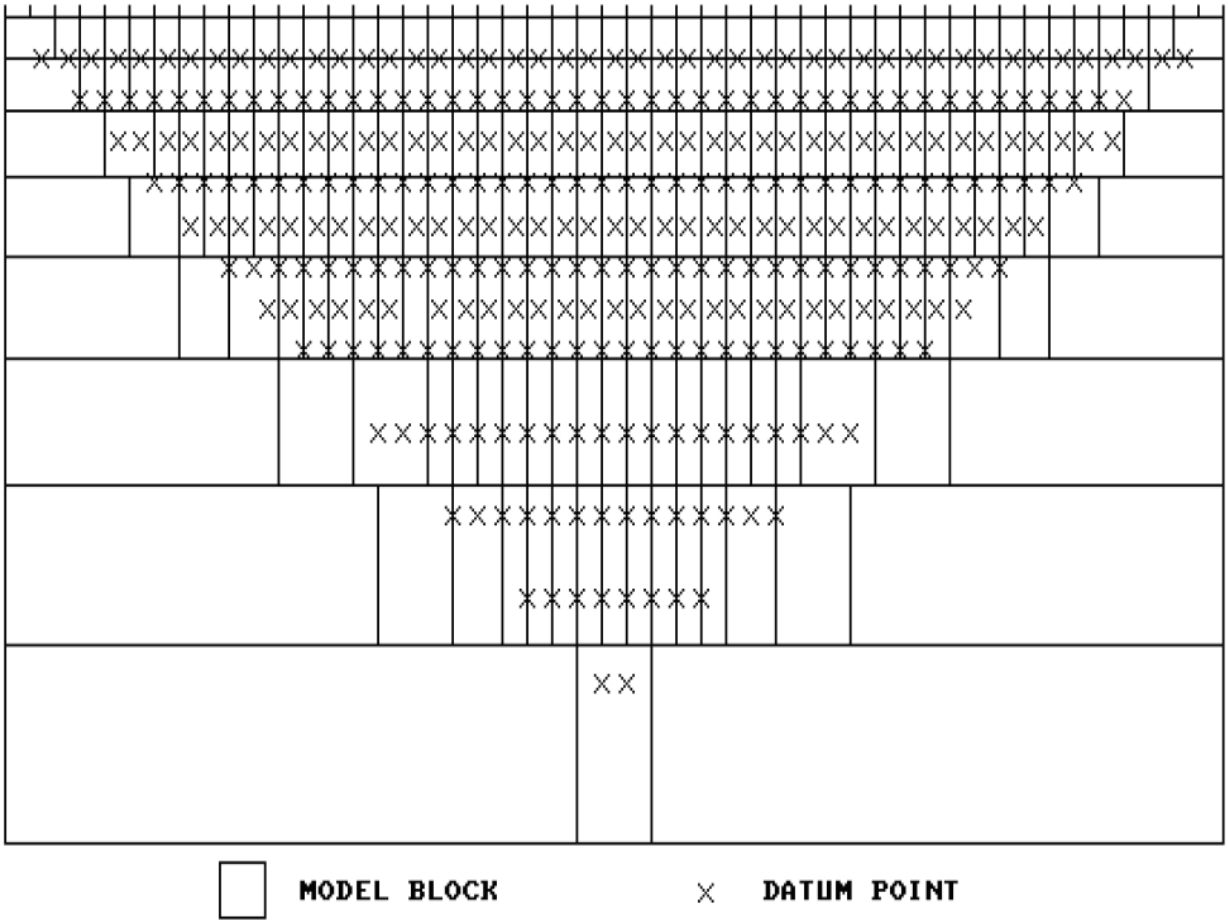



Figure 4.2 Arrangement of the blocks used in a model together with the data points in the pseudosection.

The 2D electrical resistivity images of the earth's subsurface along the profiles obtained in the study area are presented later. A total number of nine profiles were taken for this work. Five of them, profiles 1, 3, 5, 7 and 9 are along North-East to South-West direction of the survey area while profiles 2, 4, 6 and 8 are along North-West to South-East direction of the survey area (see Figure 3.4).The inversion result for each profile is also shown depicting the images of the geoelectric sections obtained from the processed data. The results show three images for each profile. The upper image is a plot of the measured apparent resistivity pseudosection which is obtained by plotting the observed apparent resistivity data against the depth with colour infill instead of line contours. The middle image is the calculated apparent resistivity pseudosection obtained by plotting the calculated apparent resistivity data against the depth with colour infill instead of line contours. The lower image is the resistivity model obtained after a definite number of iterations of the inversion programme. The resistivity model shows variation in the geologic properties of the subsurface, in relation to the measured resistivity with scales shown at the lower end of the plot, ranging from 1Ωm to 2033Ωm; the side bar shows the depth below the subsurface with a mean depth of about 17.2m and the lateral distance is shown above the section. The origin of the profiles is centred at the midpoint of each profile that is why the lateral distance of each profile starts from -40m to 40m. The negative and positive values represent distances from left and right of the midpoint respectively. The discussion of the individual profiles now follows.

### 4.3.1 Profile One

Figure 4.3 shows the measured apparent resistivity psuedosection, the calculated apparent resistivity psuedosection and the resistivity model of profile one. The resistivity model reveals a thin layer of high resistivity ranging from about 140Ωm to 787Ωm which may be composed of laterite and sand. Underlying this layer is a moderately high resistive layer to a depth of about 17.2m with resistivity value varying from about 44Ωm to 443Ωm. There is also an occurrence of small section of low resistivity between a distance on the profile of about 4m to 10m from a depth of 15m to 17.2m. This low resistivity section might be groundwater trapped in the aquifer. Although no borehole data was used to correlate the results because there was no borehole around the study area, reference was made to typical resistivities values of geological materials.

### 4.3.2 Profile Two

Figure 4.4 shows the measured apparent resistivity psuedosection, the calculated apparent resistivity psuedosection and the resistivity model of profile two. The resistivity model reveals a layer with resistivity values ranging from about 66Ωm to 361Ωm with a thickness of about 5m. This layer may be intercalation of sandy and lateritic clay which constitutes the top soil. Underlying the top soil to a depth of about 11m between the distance of -34m to -24m along the profile is a low resistivity section with resistivity values ranging from about 5Ωm to 28Ωm. The low value of the resistivity is an indication that the layer may be saturated with water. There is occurrence of high resistivity values of 361Ωm to 843Ωm between 16m to 30m and 4m to 8m on the profile, at a depth of about 4.2m and 16.5m respectively. The high resistive section is likely to be a coal seam dipping Northeast-Southwest direction, because coal is attributed with high resistivity.

NS SW

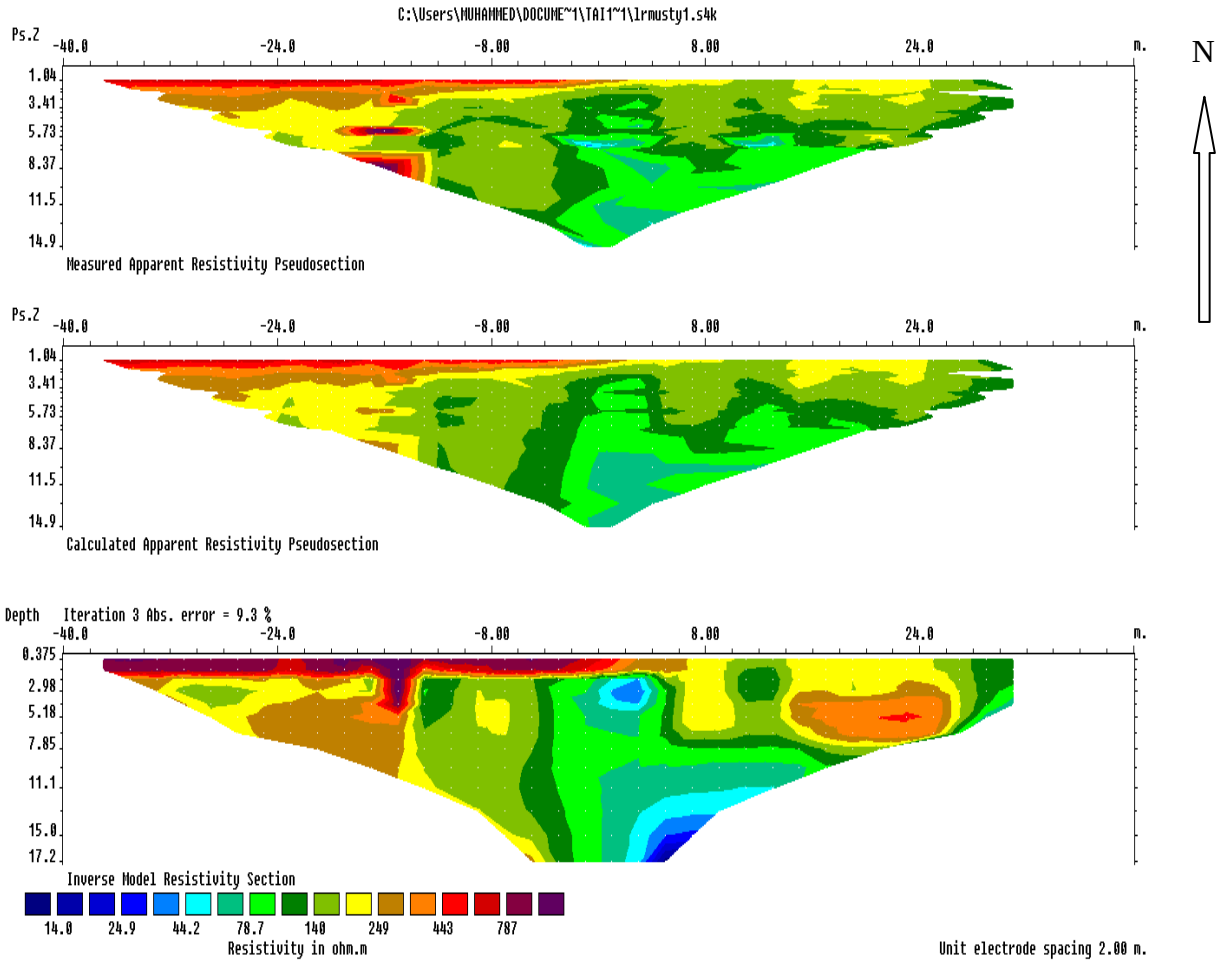



Figure 4.3: Result of 2D inversion of the Wenner-Schlumberger array data along profile 1

NW SE

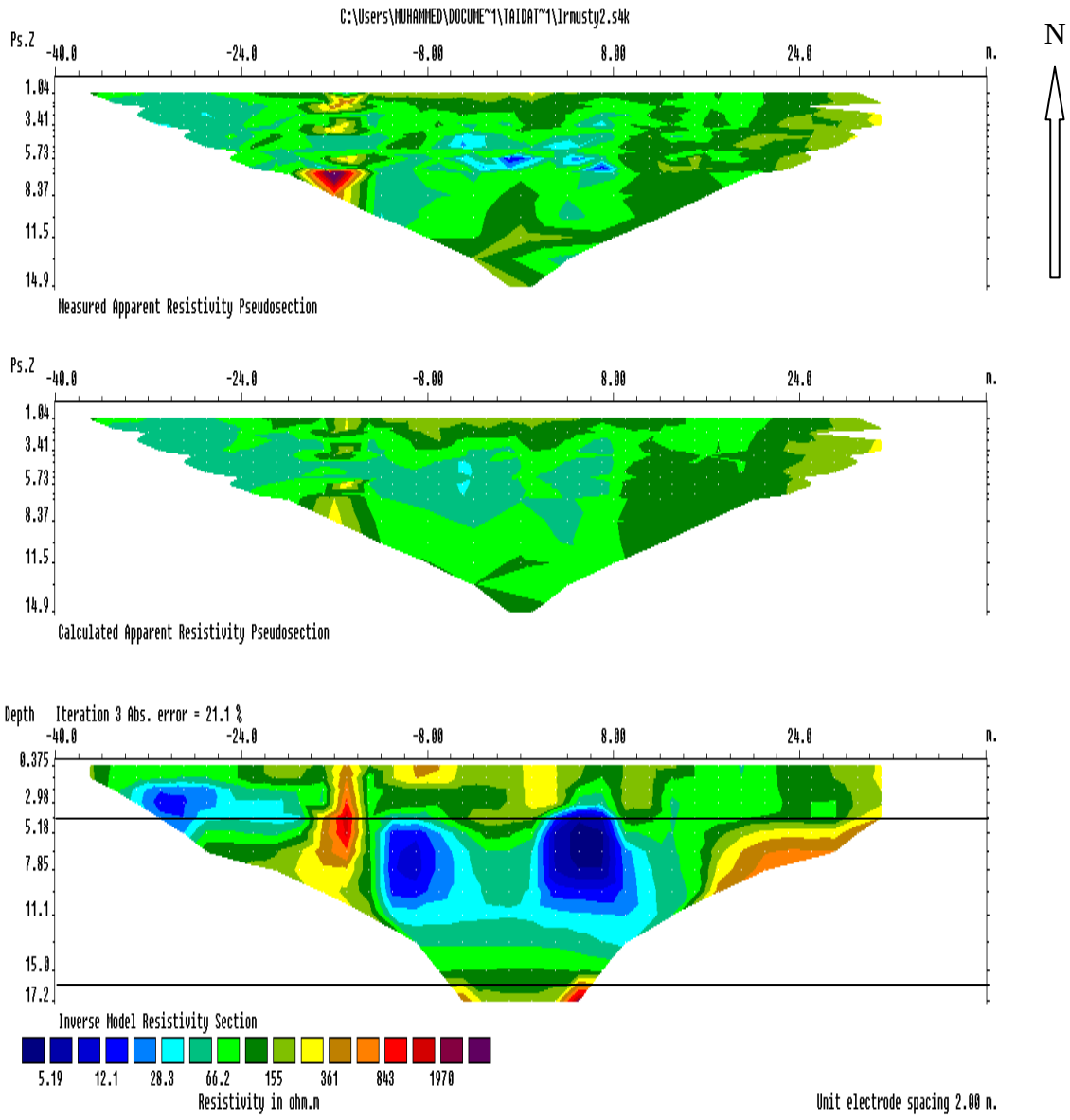



Figure 4.4: Result of 2D inversion of the Wenner-Schlumberger array data along profile 2

### 4.3.3 Profile Three

Figure 4.5 shows the measured apparent resistivity psuedosection, the calculated apparent resistivity psuedosection and the resistivity model of profile three. The resistivity model shows a high resistivity of about 113Ωm to about 396Ωm in the image and constitutes the top soil having a thickness of about 1.5m. This layer may be made up of silt, clay and sand. At a depth of about 3m to 9m, very low resistivity values of 4Ωm to 17Ωm were observed which indicate probably its clay saturated with water. Between -8m to 16m along the profile, emerge a high resistivity section with resistivity value ranging from about 212Ωm to 396Ωm at a depth of 5m to 17.2m which is suspected to be a coal seam because coal is attributed with high resistivity.

### 4.3.4 Profile Four

Figure 4.6 shows the measured apparent resistivity psuedosection, the calculated apparent resistivity psuedosection and the resistivity model of profile four. The resistivity model shows a thin layer of resistivity ranging from about 171Ωm to 309Ωm and thickness of 2m. This layer is the top soil which may be composed of sand, silt and clay. A low resistivity section occurs below the top soil with patches of very low resistivity (8Ωm to 29Ωm) between distance on the profile of -36m to -20m, -6m to 0m and 4m to14m within a depth of 2.5m to 5m and 8m to 15m. There is also appearance of high resistivity section (171Ωm to 558Ωm) between 16m to 30m and 4m to 8m along the profile at a depth of about 4m and 16.5m respectively. This high resistive section is likely to be a coal seam dipping Northeast-Southwest direction.

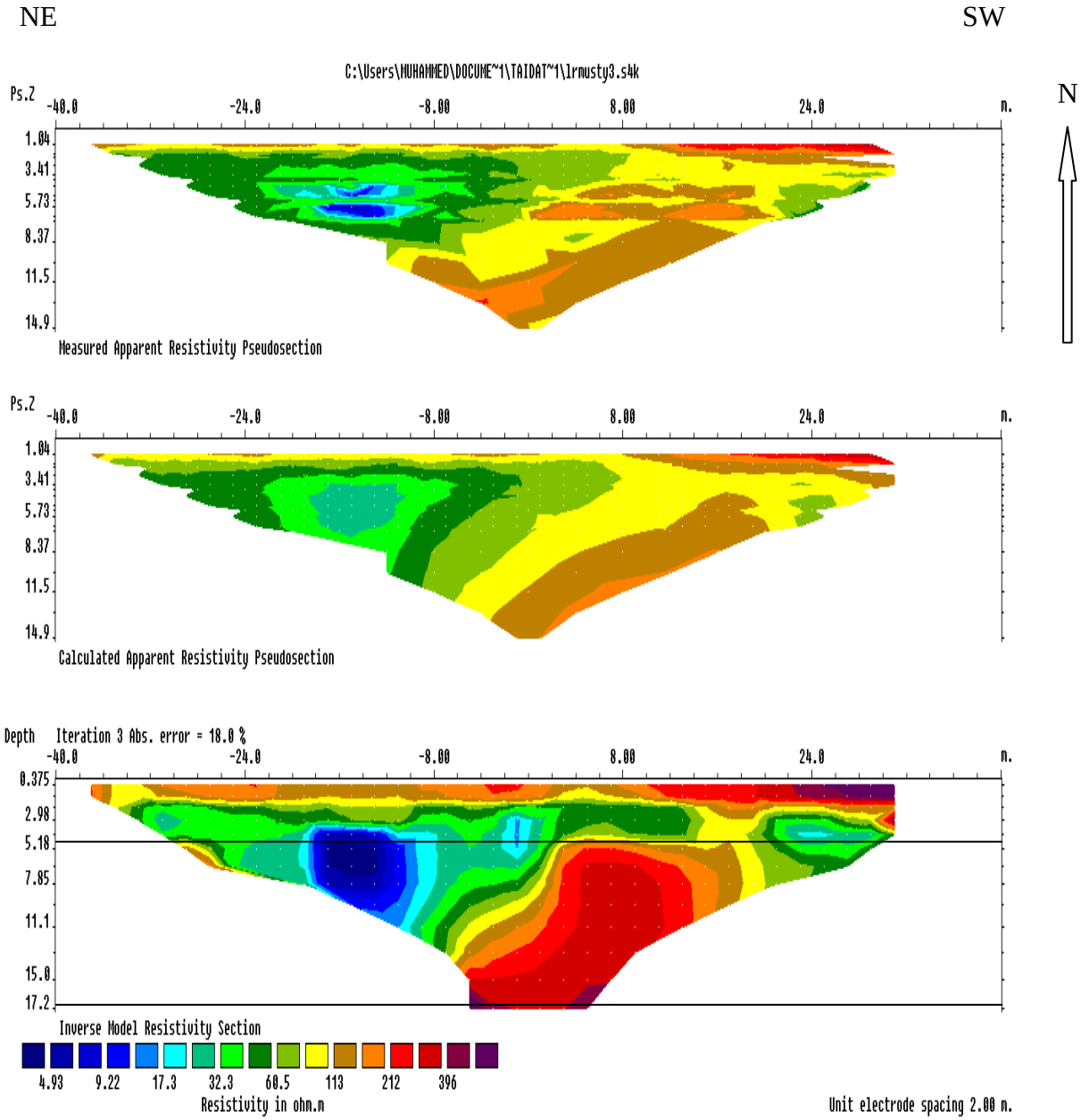



Figure 4.5: Result of 2D inversion of the Wenner-Schlumberger array data along profile 3

NW SE

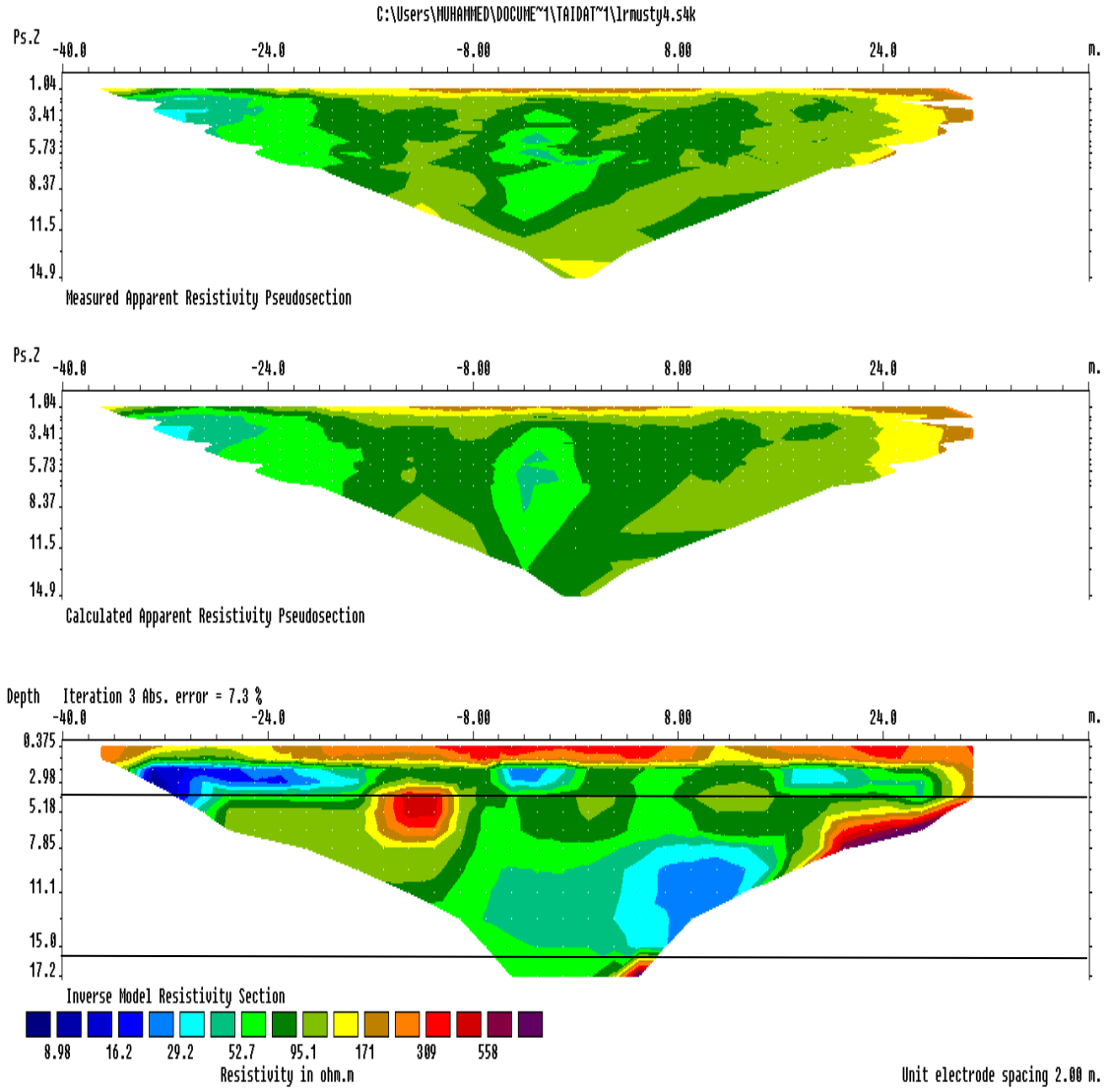



Figure 4.6: Result of 2D inversion of the Wenner-Schlumberger array data along profile 4

### 4.3.5 Profile Five

Figure 4.7 shows the measured apparent resistivity psuedosection, the calculated apparent resistivity psuedosection and the resistivity model of profile five. The resistivity model reveals a thin layer of high resistivity with resistivity value ranging from about 225Ωm to 457Ωm on the top soil which indicates the likely presence of consolidated sand, silt and clay. Between distance of -32m to -16m along the profile shows very low resistivity values 6Ωm to 13Ωm. This might probably be clayey soil saturated with water. Below the top soil is a layer with low resistivity varying from about 3Ωm to 111Ωm with a thickness of about 15m. Other isolated patches of high resistivity section ranging from 225Ωm to 457Ωm traversed by the profile are seen at -22m to -12m, -2m, 6m, and 20m to 26m marks at a depth of about 3m and 16.5m. These patches are suspected to be coal seams, since coal is associated with high resistivity.

### 4.3.6 Profile Six

Figure 4.8 shows the measured apparent resistivity psuedosection, the calculated apparent resistivity psuedosection and the resistivity model of profile six. The resistivity model reveals that the top soil is composed of consolidated sand, silt and clay having a resistivity range of 143Ωm to 379Ωm. The layer has a thickness of 2.8m. The first layer is overlain by a layer of low resistivity (20Ωm to 53Ωm) which is suspected to be an aquifer zone with a thickness of 14.4m. This implies that the basement is far, probably that might be the reason why the hand-pump borehole was sited near the location where profile six was taken. Hence, it can be inferred that the coal seam might be at greater depth.

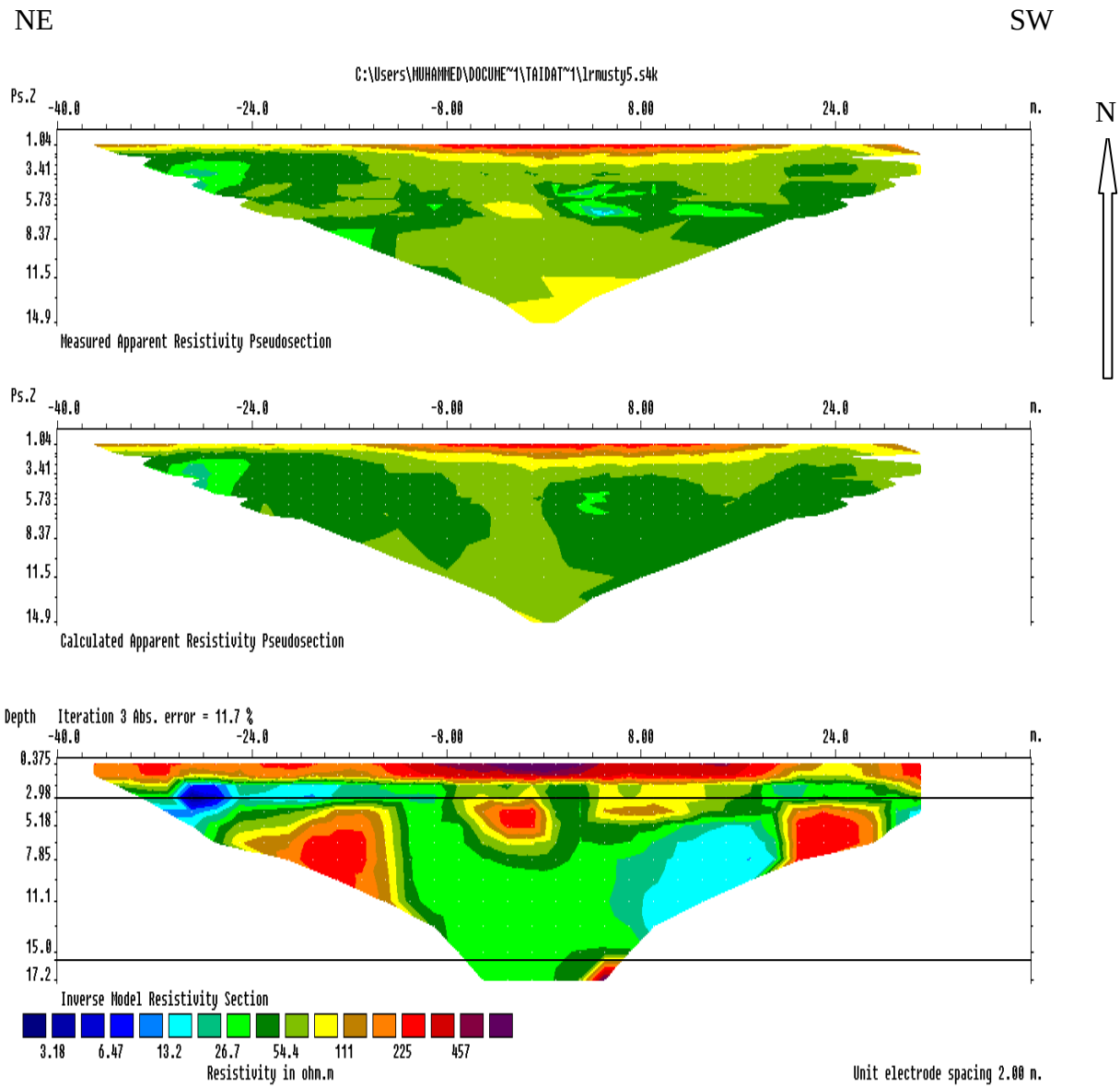



Figure 4.7: Result of 2D inversion of the Wenner-Schlumberger array data along profile 5

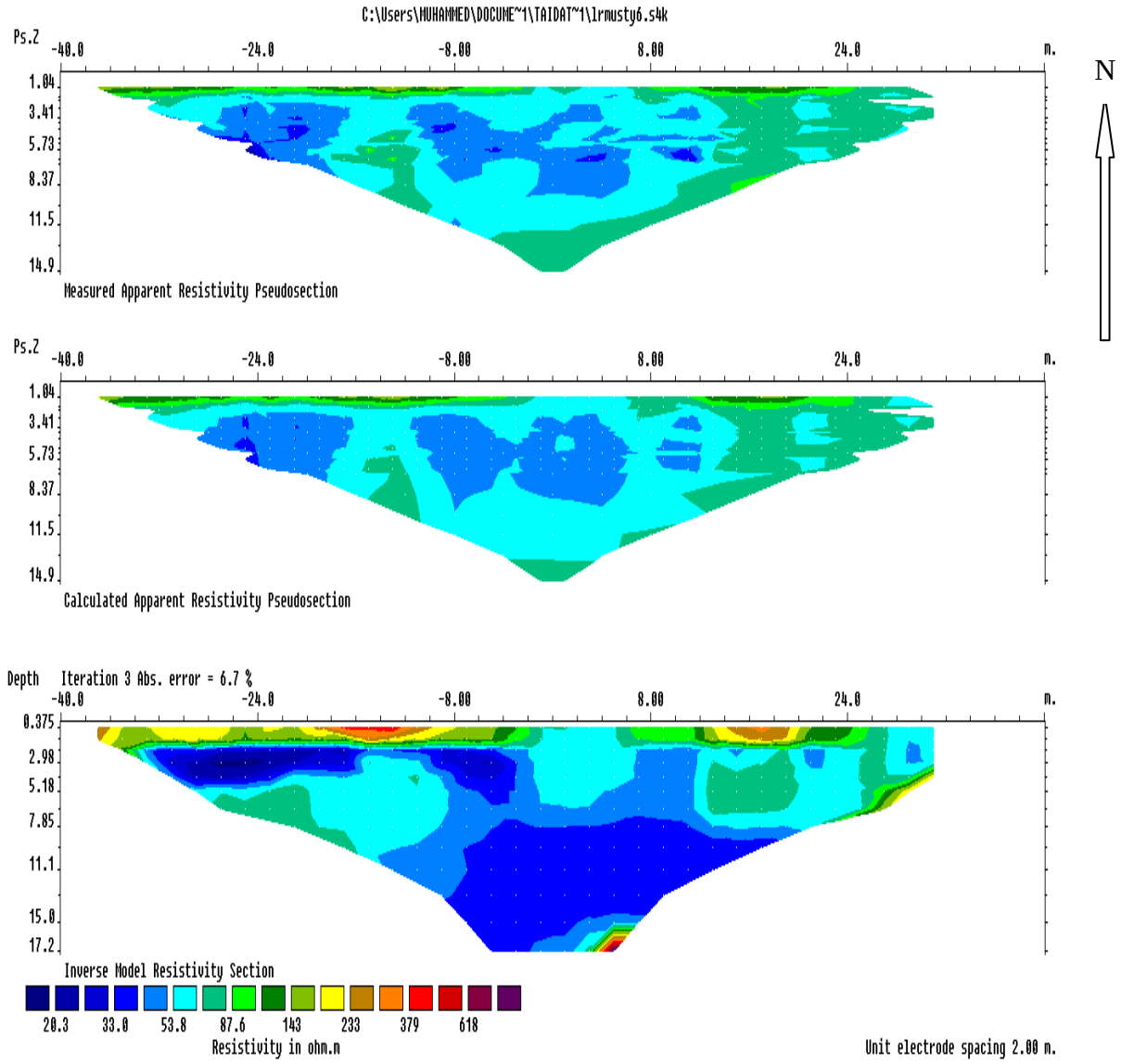



Figure 4.8: Result of 2D inversion of the Wenner-Schlumberger array data along profile 6

### 4.3.7 Profile Seven

Figure 4.9 shows the measured apparent resistivity psuedosection, the calculated apparent resistivity psuedosection and the resistivity model section of profile seven. The resistivity model section shows a thin layer which may be intercalation of sandy and lateritic clay as the top soil with resistivity ranging from about149Ωm to 280Ωm and thickness of about 1m. Underlying this layer is a low resistivity value of about 30Ωm to 57Ωm. The low resistivity value of the layer is an indication that it may be saturated with water since the resistivity of a rock decreases as the percentage of water saturation increases. There is no indication of the presence of coal from the inverse resistivity model. If at all it may exist here, then it might be at a greater depth.

### 4.3.8 Profile Eight

Figure 4.10 shows the measured apparent resistivity psuedosection, the calculated apparent resistivity psuedosection and the resistivity model of profile eight. The resistivity model shows patches of high resistivity ranging from about 404Ωm to 907Ωm on the surface which constitutes the top soil that is composed of mainly dry sand. The top soil has high resistivity because its pore space lacks water. Directly underlying this layer may be a clay layer with low resistivity values ranging from about 7Ωm to 35Ωm. The low resistivity zone indicates that water is probably trapped within the layer. This resistivity model also indicated that the basement is far. The possibility of intercepting a coal seam here might be at greater depth.

NE SW

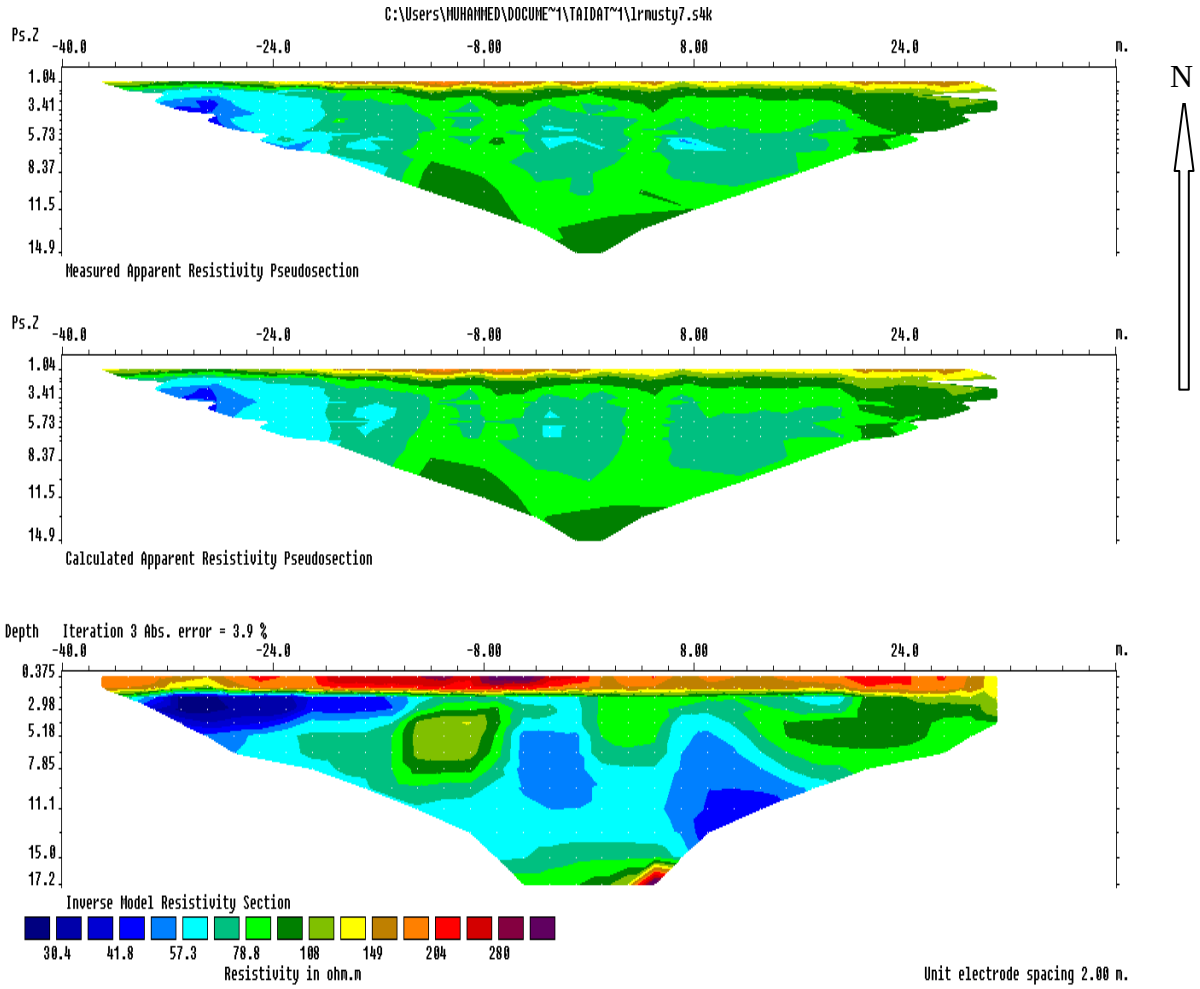



Figure 4.9: Result of 2D inversion of the Wenner-Schlumberger array data along profile 7

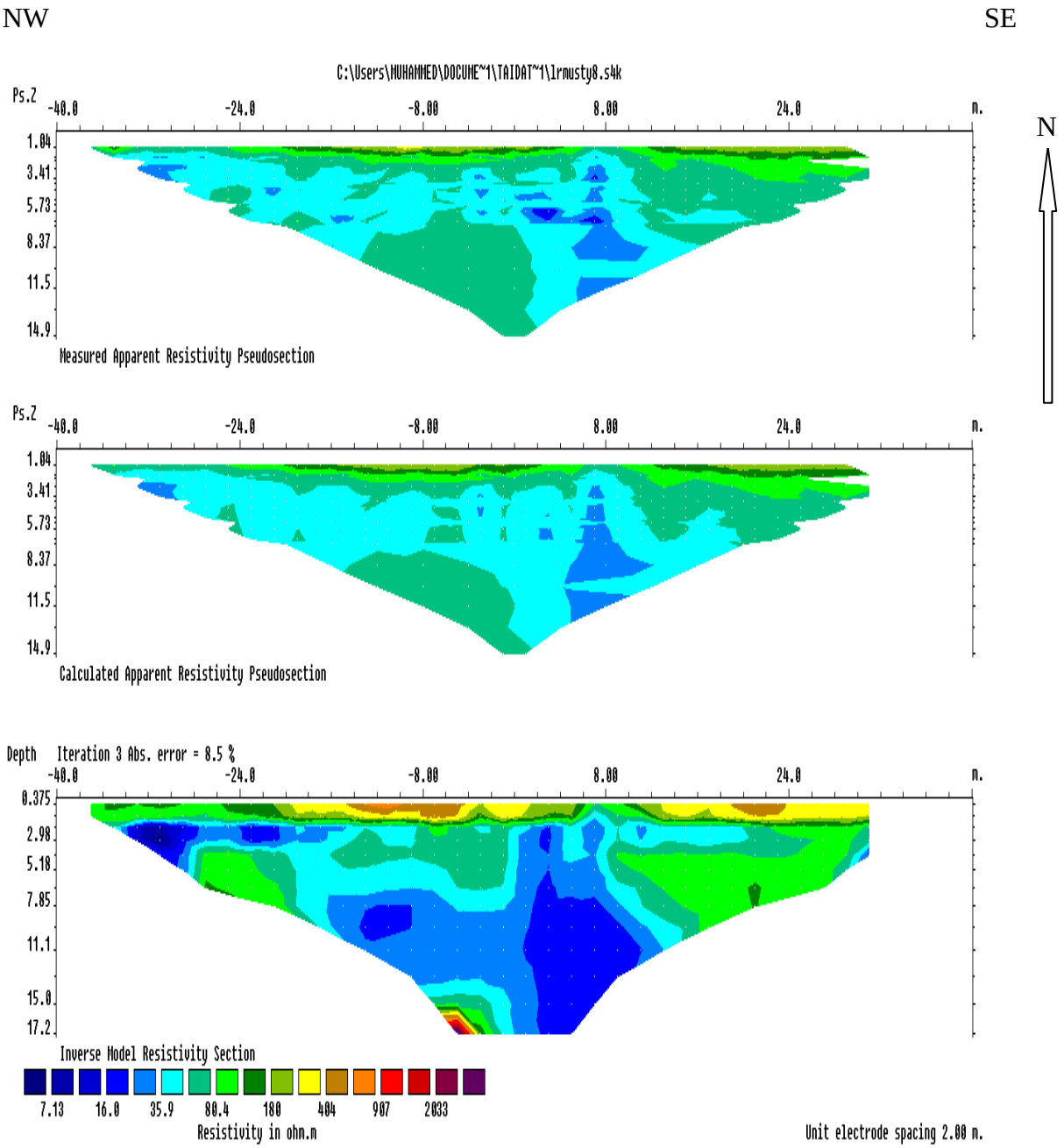



Figure 4.10: Result of 2D inversion of the Wenner-Schlumberger array data along profile 8

### 4.3.9 Profile Nine

Figure 4.11 shows the measured apparent resistivity psuedosection, the calculated apparent resistivity psuedosection and the resistivity model of profile nine. The resistivity model shows the top soil with resistivity values ranging from about 83Ωm to 365Ωm and a thickness of about 1.5m. This is likely due to the observed dry and consolidated lateritic clay top soil. Underlay the top soil is a low resistivity section with resistivity values ranging from about 27Ωm to 57Ωm. The section might probably be groundwater trapped in an aquifer. At a depth of about 3.8m to17.2m, there is occurrence of very high resistive section ranging from about 174Ωm to 365Ωm which might be a coal seam at a shallow depth.

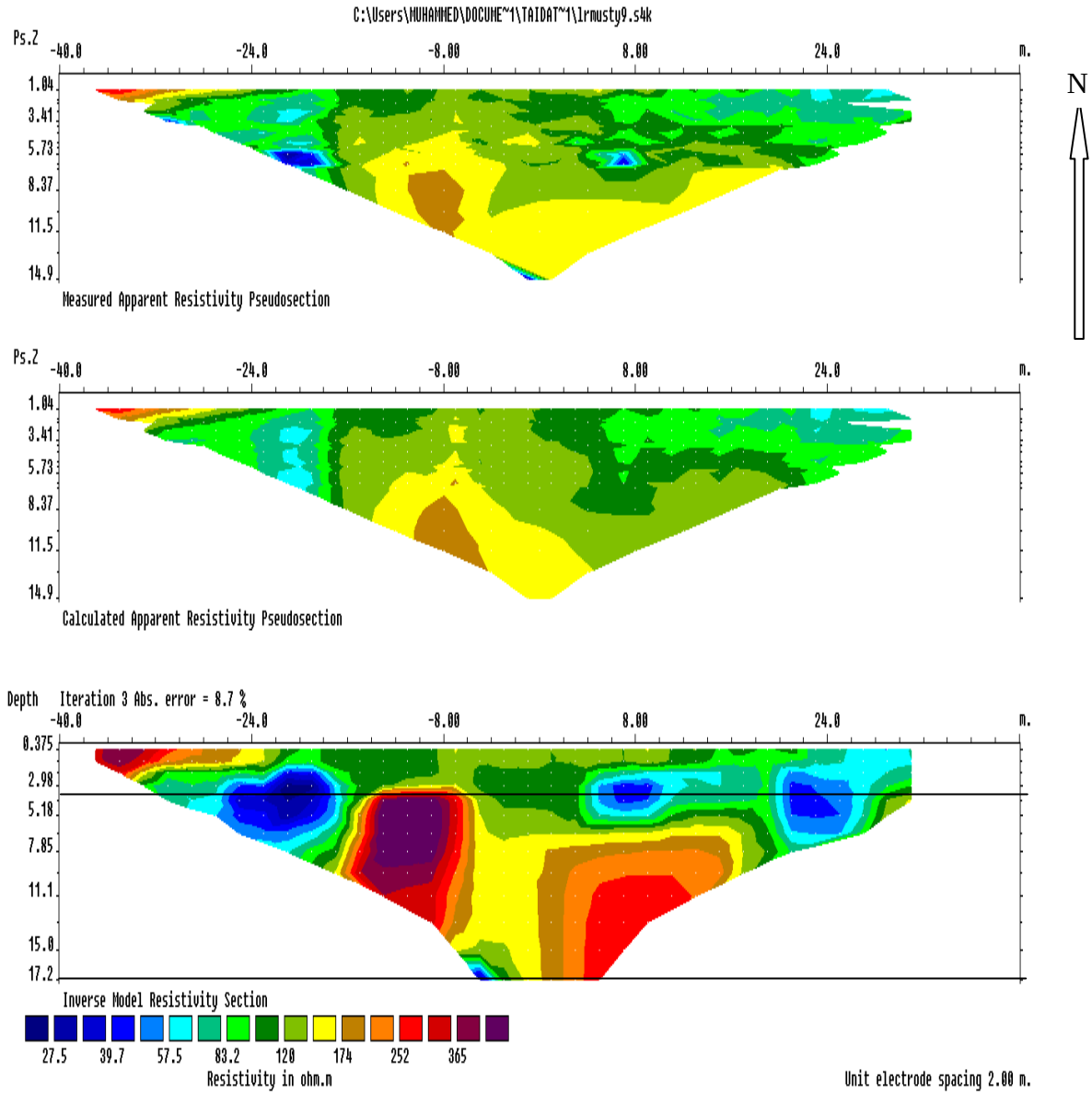



Figure 4.11: Result of 2D inversion of the Wenner-Schlumberger array data along profile 9

### 4.4 Merging of the profiles for the detection of continuity of the subsurface structures

The resistivity model of each profile taken was aligned as in the map illustrating the profiles layout (see Figure 4.12). This is done to enable the check for continuity of the subsurface structures.

**Continuity of structures**: It is assumed that structures or stratum cannot end abruptly within a basin of deposition, but must feather out, or extend across the width of the basin and terminate against older rocks. According to Steno's Principle of lateral continuity "Material forming any stratum was continuous over the surface of the earth unless some other solid bodies stood in the way (Stovall, 1955)." The principle of lateral continuity has application to the correlation of strata. Where the lateral continuity of the strata is missing, erosion or faulting can be inferred. In his words: "If a body or discontinuity cuts across a stratum, it must have formed after that stratum (Stovall, 1955)." This principle is used to trace coal seams from one mountain to the next in West Virginia.

A careful look at Figure 4.12, proved the authenticity of the data because it shows continuity of the geological structures. For instance the suspected coal seam in profile 4 extends to profiles 2 and 3. Likewise in profile 8, the suspected clay saturated with water extends to profiles 6 and 7.

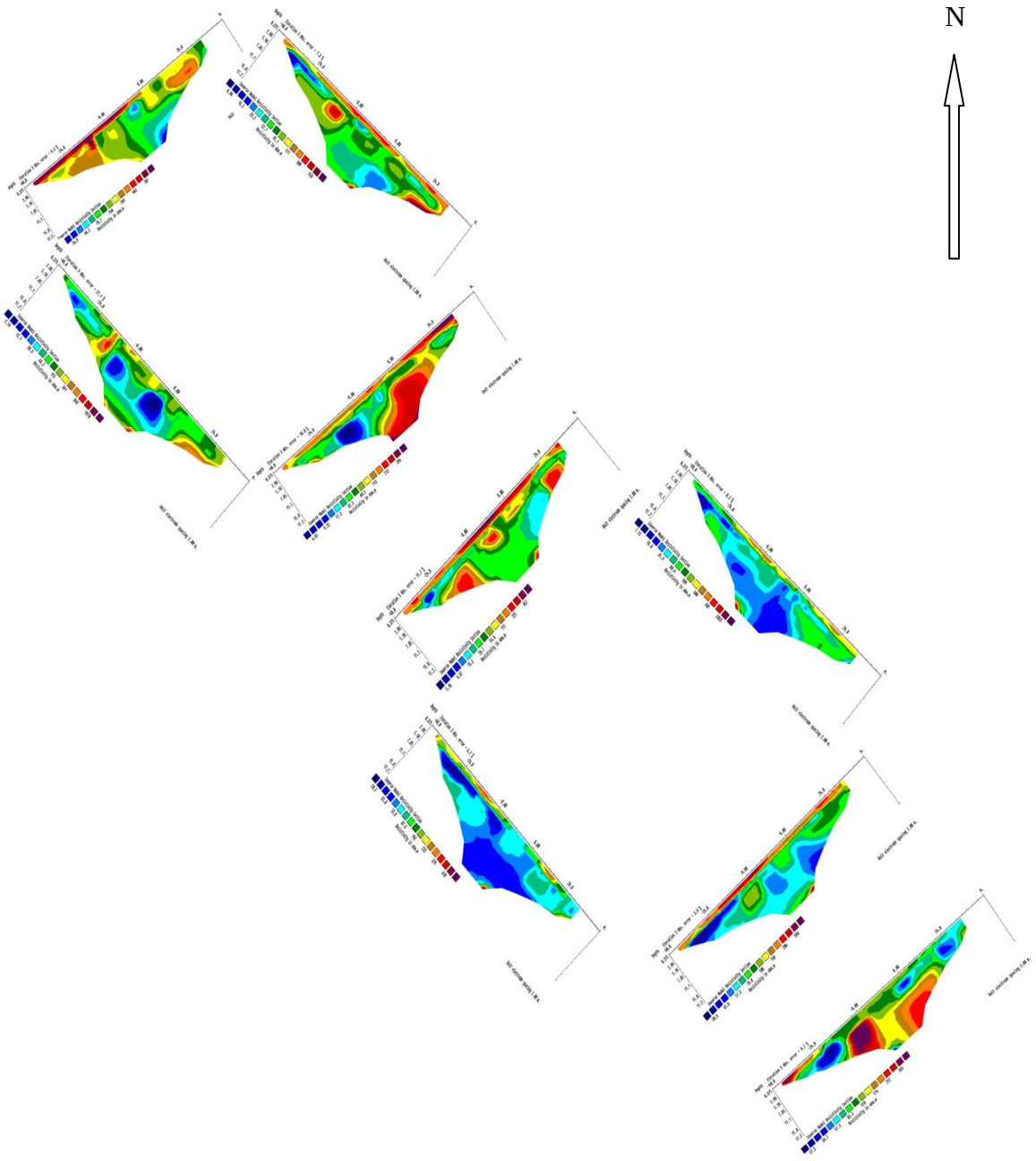



Figure 4.12 Resistivity model sections of all the profiles

# CHAPTER FIVE: DISCUSSION, CONCLUSIONS AND RECOMMENDATIONS

## 5.1 Discussion

The resistivity values of the subsurface structures obtained in this research lies between 3Ωm to about 2033Ωm. It indicates variation of subsurface material/soil based on grain size, porosity and permeability of the layer. In almost all of the nine resistivity models obtained, the top soil appears to have moderately high resistivity varying from 66Ωm to 907Ωm which extend to a thickness of about 2.5m from the surface. Below the top soil comes a layer with low resistivity whose values ranges from about 3Ωm to 57Ωm indicating that the layer might be saturated with water.

All the nine profiles were aligned (Fig. 4.12) as they were taken during the survey (see Fig. 3.5) so as to observe the geologic trend of the possible occurrence of coal seams. It can be observed from the four profiles that were taken surrounding point P1 (location of the hand dug well), that there are high resistivity sections with resistivity values ranging from about 361Ωm to 1970Ωm for profile 2 and 250Ωm to 558Ωm for profile 4. These high resistivity sections occur in both profiles between a distance of 16m to 30m and 4m to 8m on the profile at a depth of about 7m and 17.2m indicating continuity in the subsurface structures. Though, basement rock is also characterized with high resistivity, but its resistivity is higher than that of coal. Based on this, it can be inferred that this high resistive section might be that of a coal seams since its resistivity value range from about 250Ωm to 900Ωm. A close look at profile 3 reveals that the profile was laid parallel to the suspected strike of the coal seam. That is why the high resistive section (suspected coal seams) is observed to be elongated. It is likely to represent the coal seams observed in profile 2 and 4 that extends towards profile 3. Since profile 2 and 4 were taken perpendicular to the

suspected coal seams it therefore gives a clearer picture of where the coal seam is striking. Hence it can be observed that the coal seam is striking in Northeast-Southwest direction.

Similarly, from the resistivity models of the four profiles taken around and surrounding point P2 (location of the hand-pump borehole), it can be seen that the continuity observed previously still persisted with the top soil having high resistivity indicating most likely the presence of sand. Below the top soil is a very low resistivity section with resistivity values ranging from 7Ωm to 90Ωm, which is an indication that the basement is deeper within this region. This might have coincided with the previous survey that was probably used in locating the position of the hand-pump borehole, since the position is favoured by a large overburden thickness. Therefore the coal seam is suspected to be at a deeper depth here. A close look at profile 9 indicates the occurrence of high resistive section which implies the likely reappearance of the coal seam at a shallower depth.

### 5.2 Conclusions

Electrical resistivity imaging was successfully carried out at Tai/Akko area of Gombe State, Northeastern Nigeria with the aim of delineating the lateral extent of the coal deposit, the strike direction and the resistivity values associated with the coal seam. The results of the electrical resistivity imaging showed that the near surface materials may be composed of sand and laterite with resistivity values ranging from about 150Ωm to 400Ωm. Below the near surface materials, is a layer likely to be clay saturated with water. It was more pronounced in profiles 6 and 8 which have low resistivity values of about 3Ωm to 50Ωm. Underlying the clay layer in profiles 2, 3 and 4, was a high resistive zone with resistivity values ranging from about 250Ωm to 900Ωm and depth varying from 7m to

17.2m. This high resistivity is too low to be that of the basement rock and is therefore inferred to be a coal seam. There is also likely occurrence of the coal seam at a shallower depth in profiles 9 due to the reappearance of high resistivity which is similar to that of profiles 2, 3 and 4 located near the hand dug well where coal had been intercepted. Based on these results, it can be concluded that the occurrence of the coal seam is probably more at the Northwest of the survey area and the coal seam is suspected to have resistivity values ranging from about 250Ωm to 900Ωm. It can also be inferred that the coal seam is striking in the Northeast-Southwest direction.

### 5.3 Recommendations

Based on the result of this research, it is recommended that:-

Further investigation should be carried out on the profiles using equipment with wider electrode spacing so that it will probe deeper into the subsurface.

Seismic method can also be used so as to compliment results obtained from the resistivity investigation.

## REFERENCES


ABEM Instrument AB (2010). Terrameter SAS1000/4000 LUND Imaging System Instruction Manual.

Akande, S. O., Ojo O. J., Erdtmann, B. D., Hetenyi, M. (1998). Paleoenvironments, source rock potential and thermal maturity of the upper Benue rift basins, Nigeria. Implications for hydrocarbon exploration. *Organic Geochemistry*, **29**: 531–542.

Apparao, A. and Roy, A. (1971). Resistivity model experiments. Geoexploration, **7**: 45-54.

Bhattacharaya, P. K. and Patra, H. P. (1968). Direct current geoelectrical soundings. *Elsevier, Amsterdam*, pp 70-91.

Batayneh, A. T. (2006): Resistivity Tomography as an aid to planning gas pipeline construction, Risha Area, North-East Jordan. *Near Surface Geophysics,* Vol. **4**, pp. 313 – 319.

BGR, (2009). (Bundesanstalt fur Geowissenschaften und Rohstoffe – Federal Institute for Geosciences and Natural Resources), *Reserves, Resources and Availability of Energy Resources – Annual Report 2009*, BGR, Hannover, Germany, www.bgr.bund.de.

C.E.C.,California Energy Commission (2012). Energy Story; Chapter 8: Fossil Fuels - Coal, Oil and Natural Gas. Retrieved from http://www.energyquest.ca.gov/story/chapter08.html.

Cardarelli, E. and Fischanger, F. (2006). 2D data modelling by electrical resistivity tomography for complex subsurface geology. *Geophysical Prospecting*, Vol. **54**. Pp. 121 – 133.

C.I.A.B.,Coal Industry Advisory Board (2008). Clean Coal Technologies: Accelerating Commercial and Policy Drivers for Deployment, CIAB, International Energy Agency, Paris.

Dahlin, T. (2001). The Development of Electrical Imaging Techniques. *Computers and Geosciences,* **27**(9), 1019-1029.

de Groot-Hedlin, C. and Constable, S., (1990). Occam's inversion to generate smooth, two-dimensional models form magnetotelluric data. *Geophysics,* **55**, 1613-1624.

Edwards, L.S., (1977). A modified Pseudosection for Resistivity and Induced Polarization. *Geophysics*, **42**, 1020 – 1036.

Ehinola, O. A., Oluwajana A. and Adekoya A. T. (2012). Geophysical investigation and reserve estimation of a coal seam in Ute area, southwestern Nigeria. *Petroleum & Coal,* **54**(3): 252-259.

Ewing, M. A., Crary, A. P. Peoples J. W. and Peoples, J. A. (1936). Prospecting for Anthracite by the Earth Resistivity Method. *Transactions of the American Mining and Metallurgical Engineers,* Coal Division, Vol. **119**, pp 43-483.

Griffiths, D. H., Turnbull, J. and Olayinka, A. I. (1990). Two-dimensional resistivity mapping with a computer-controlled array. First Break, Vol. **8** (4), Pp. 121 – 129.

Johnson, W.J., Appolonia D., and Monroeville, P.A. (2003). Applications of the electrical resistivity method for detection of underground mine workings. Geophysical Technologies for Detecting Underground Coal Mine Voids, Lexington, Kentucky.

Kean, W. F., Muriel, J. W. and Richard, L. H. (1987). Monitoring moisture migration in the vadose zone with resistivity. *Groundwater*, v.**25**, No.5, pp.562-571.

Keller, G. V. and Frischknecht, F. C., (1966). Electrical methods in geophysical prospecting. Pergamon Press, pp. 20 – 31.

King, M. H., (2014). Coal. Retrieved from http://geology.com/rocks/coal.shtml

Koefoed, O., (1979). Geosounding Principles, 1: Resistivity sounding measurements. *Elsevier press.*

Krishnamurthy, N.S., Rao, A.V., Kumar, D., Singh, K.K.K. and Ahmed, S. (2009). Electrical Resistivity Imaging Technique to Delineate Coal Seam Barrier Thickness and Demarcate Water Filled Voids. *Journal of Geological Society of India* **73**: 639-650.

Kumar, R. (1973). Resistivity type curves over outcropping vertical dyke-I. *Geophysics Prospect*, **21**:560-578.

Loke, M.H., (1994). The inversion of two-dimensional resistivity data. Unpubl. PhD thesis,University Of Birmingham.

Loke, M. H., (1999). Electrical imaging surveys for environmental and engineering studies; a practical guide to 2-D and 3-D surveys. Self Published Note Book, 15-57.

Loke, M.H. (2004). *Tutorial: 2-D and 3-D Electrical Imaging Surveys*. Retrieved from http://www.geotomosoft.com

Loke, M.H. (2014). *Tutorial: 2-D and 3-D Electrical Imaging Surveys*. Retrieved from http://www.geotomosoft.com

Loke, M. H. and Barker R. D., (1996). Rapid least-squares inversion of apparent resistivity pseudosections using a quasi-Newton method. *Geophysical Prospecting,* **44**, 131 – 152.

Long, O. (1954). Mapping nearly vertical discontinuities by earth resistivity, *Geophysics (USA),***19**: 739-760.

M.M.S.D., Ministry of Mines and Solid Mineral Development (2010). Coal Exploration and Power generating opportunities in Nigeria. Retrieved from www.resourcedat.com > uploads > 2011/11.

Nwaobi, G. C. (2005). "The Nigerian Coal Corporation: An Evaluation of Production Performance (1960-1987)". Retrieved 2008-04-12.

Obaje, N.G. (2009). *Geology and Mineral Resources of Nigeria, Lecture Notes in Earth Sciences Springer-Verlag Berlin Heidelberg,* pp. 57-68.

Oladapo, M.I., Adeoye, O.O., and Alao, T.O. (2008). Geoelectric Study of Coal Deposits at Unwana/Afikpo Area of Southeastern Nigeria. *Journal of Applied Sciences Research,* **4**(11): 1534-1545.

Oldenburg, D.W. and Li, Y. (1999). Estimating depth of investigation in D.C. Resistivity and IP surveys. *Geophysics*, Vol. **64** (2), Pp. 403-416.

Pattela, D. (1978). Resistivity sounding on a multi-layered earth with transitional layers, Part-II: Theoretical and field examples. Geophysics Prospecting, **26**: 130-156.

Pazdirek, O. and Blaha, V. (1996). Examples of resistivity imaging using ME-100 resistivity field acquisition system. *European Association of Geoscientists and Engineers (EAGE) 58th Conference and Technical Exhibition Extended Abstracts, Amsterdam.*

RES2DINV ver.3.59 (2010). Geoelectrical Imaging 2D and 3D *Geotomo Software.* Malaysia. February 2010. Retrieved from www.geoelectrical.com

Sada, M.M. (2012). Investment opportunities in Nigerian mineral and metal sector. Paper presented at Africa Down Under International Conference, Perth, Western Australia.

Sasaki, Y. (1992). Resolution of resistivity tomography inferred from numerical simulation. *Geophysical Prospecting*, **40**, 453-464.

Sheets, R. A. (2002). Use of Electrical Resistivity to Detect Underground Mine Voids in Ohio In: Water-Resources Investigations Report 02-4041.

Simon, D. (1995). Coal 'First used in Iron Age' British Archaeology. Retrieved from http://www.britarch.ac.uk/ba/ba2/ba2news.html.

Singh, K. K. K., Singh, K. B., Lokhande, R. D. and Prakash, A. (2004). Multielectrode resistivity imaging technique for the study of coal seam in northern part of Jharia Coalfield of Dhanbad district. *Journal of Scientific and Industrial Research,* **63**: 927-930.

Stanley, W. D.,Jackson D. B and Zohdy A. A. R. (1976). Deep electrical investigations in the valley geothermal area, California. *Geophysics Prospecting,* **81**: 810-820.

Stovall, J. W. (1955). The Principle of Historical Geology. Retrieved from pages.geo.wvu.edu/~kammer/g231/Principles.pdf.

Telford, W. M., Geldart, L. P., Sheriff, R.E. and Keys, D.A., (1976). *Applied Geophysics.* Cambridge University Press, London, pp. 860-870.

Telford, W.M., Geldart, L. P. and Sheriff, R. E. (1990). *Applied Geophysics* second edition. Cambridge University Press, London, pp. 522-525.

U.S.D.E.,United States Department of Energy (2003). Fossil Energy. Retrieved from http://www.fe.doe.gov/education/energylessons/coal/coal_history.html.

World Coal Institute (2009). *The coal resources: A comprehensive overview of coal* (Research report). Retrieved from http://www .worldcoal.org

Zaborski, P. M., Ugoduluwa, F., Idornigie, A., Nnabo, P. and Ibe, K. (1997). Stratigraphy and structure of the Cretaceous Gongola Basin, north eastern Nigeria. *Bulletin des centres des Recherches Exploration-production Elf- Aquitaine,* **21**: 153-185.

Zohdy A. A. R. (1969). The use of Schlumberger and equatorial soundings in groundwater investigations near EI Paso, Texas, *Geophysics (USA),* **34**: 713-728.